CALSPAN UB RESEARCH CENTER

DEVELOPMENT OF AN INTEGRATED BEM APPROACH FOR HOT FLUID STRUCTURE INTERACTION

ANNUAL REPORT

NOVEMBER 1986 - NOVEMBER 1987

Gary F. Dargush
Prasanta K. Banerjee
Department of Civil Engineering
State University of New York at Buffalo

Michael G. Dunn
Calspan Corporation

LIST OF CONTENTS

1. INTRODUCTION

Significant advances in present state-of-the-art analytical and experimental techniques are required to improve both the durability and reliability of hot section Earth-to-orbit engine components. These components, directly in the hot gas flow path, are subjected to severe thermal and mechanical loadings which can lead to creep-enhanced distortion and low-cycle fatigue. As operating temperatures are pushed higher and as more demanding applications, such as the space shuttle main engine and future Earth-to-orbit propulsion systems, are attempted, the environment in which the hot section components must survive becomes even more severe, and the effects of interaction between these components and the hot gas becomes significant. Consequently, the development of increasingly durable, structurally-efficient designs will benefit from the use of enhanced analytical techniques capable of producing reliable stress, deformation, and temperature profiles for the combined fluid-structure problem. An analysis of these type of problems requires the combined use of solid mechanics, fluid mechanics and heat transfer theories.

This report details progress made, during the period November 1986 - November 1987 in a three-year program commencing in March 1986, toward the development of a boundary element formulation specifically designed for the study of hot fluid-structure interaction in Space Shuttle Main Engine (SSME) hot section components. The primary thrust of the program to date has been directed quite naturally toward the examination of fluid flow, since boundary element methods for fluids are at a much less developed state. During the first year, work focused on the completion of a comprehensive literature review of integral methods in fluids, the development of integral formulations for both the solid and fluid, and some preliminary infrastructural enhancements to a boundary element code to

permit incorporation of the fluid-structure problem. However, in the second year, emphasis shifted to the implementation and validation phases.

In particular, during the past year, boundary element formulations were implemented in two-dimensions for both the solid and the fluid. The solid was modeled as an uncoupled thermoelastic medium under plane strain conditions, while several formulations were investigated for the fluid. For example, both vorticity and primative variable approaches have been implemented for viscous, incompressible flow. More recently, compressible versions have also been developed. All of the above boundary element implementations were incorporated in a general purpose two-dimensional code. Thus, problems involving intricate geometry, multiple generic modeling regions, and aribitrary boundary conditions are all supported.

In the next section, a brief review of the most recent boundary element literature for fluid flow is presented. This is followed by the development of integral formulations for the solid in Section 3 and for the fluid in Section 4. Several numerical examples are presented at the end of each of those two sections. In the latter case, this is followed by a discussion of the results and suitability of the various algorithms. The remaining sections then summarize the progress achieved to date, outline the work plan for the next year, and provide a list of references. Tables and figures appear at the end of the corresponding section.

2. LITERATURE REVIEW ON FLUIDS

Relatively little work has been done on the numerical solution of fluid flow problems for intermediate and large Reynolds numbers. Much of that work is on hybrid formulations, with integral equations used for the surfaces and finite differences or finite elements for the fluid volume. Pure integral equation formulations have the additional complexity that volume integrals enter the picture. This, in retrospect, is not a serious problem in that volume computations are restricted to those parts of the problem where viscous effects (both Newtonian and non-Newtonian cases) are significant. Furthermore, the vast majority of existing applications are simply for two-dimensional test problems. The following basic formulations are distinguished:

Velocity and Vorticity Formulations

Here pressure is replaced by vorticity, which is defined as the curl of the velocity vector. The kinematics of flow are described by a vectorial Poisson's equation. The kinetic aspects of the problem are described by the vorticity transport equation, which is a parabolic, time-dependent type of equation. Integral equation formulations for either vectorial elliptic or parabolic equations are well understood (Wu, 1976b; Banerjee and Butterfield, 1981). The coupling of these two equations, however, is a much more difficult proposition. For the general case of flow past a solid object such as an airfoil, either the velocity or the vorticity must be specified on its surface. In addition, radiation type of boundary conditions must hold for unbounded fluid domains. This formulation is especially well suited for two-dimensional problems, because the vorticity becomes a scalar.

Starting in the early seventies, Wu and his co-workers have published

extensively on their hybrid approach for time-dependent viscous flow (Wu and Thompson, 1973; Wu et al 1974; Wu, 1976a; Sankar and Wu, 1978; Wu and Rizk, 1978; Wu et al, 1984). This work is summarized in Wu (1982; 1984) and the general strategy is as follows: The integral representation of the kinematic part of the problem is by Biot-Savart's law that involves both surface and volume integrals. For the case of flow past a solid body with the frame of reference attached to that body, the surface integrals vanish and what is left is a relation between the velocity and the volume integral of the vorticity. Viscous effects are originally concentrated only around the surface of the solid body and subsequently spread to a small portion of the surrounding fluid domain. Thus, it is only necessary to discretize the boundary of the solid and the part of the volume where viscous effects are important in order to evaluate the volume integral. Since the velocity is zero at the solid surface, a relationship between vorticity at the surface and vorticity throughout the volume is obtained through nodal collocation (condition 1).

The integral representation of the kinetic part of the problem is in terms of both time and space integrations. Furthermore, space integrations include volume terms that account for the nonlinearities in the vorticity transport equations. Other than recasting this volume integral into more convenient forms, it is not in general possible to convert it to a surface integral. Standard nodal collocation then gives, at time step k, a condition involving vorticity and its spatial derivative at the surface, velocity-vorticity products throughout the volume, and the initial conditions (condition 2).

A typical solution scheme is incremental/iterative in character. From known values of the velocity and the vorticity at time step k-1 and throughout the fluid domain, condition 2 can be used to solve for the

vorticity at time step k and at all nodes not on the surface. An iterative procedure is required due to the presence of velocity times vorticity terms. Next, boundary values of the vorticity at k are found by using condition 1. Finally, interior values of the velocity at k are computed from the original kinetic condition. Boundary values of the velocity are zero for this type of problem. Using this basic type of procedure Wu and his co-workers solved a wide range of problems such as flow past a finite flat plate under zero angle of attack, flow past circular cylinders, and flow past airfoils. In earlier work, the vorticity transport equation was solved by finite differences (Wu and Thompson, 1973), finite differences with segmentation of the flow field (Wu et al, 1974), finite elements (Wu et al, 1978a), and finite Fourier series in conjunction with the integral representation in a conformally transformed plane (Wu and Sugavanam, 1978).

A similar approach was independently proposed by Coulmy (1976). At first, the panel method is used for the numerical solution of the integral equation for kinematics. This allows for expressing the velocity in terms of the vorticity. Subsequently, the vorticity is computed in an iterative fashion from finite differencing of the vorticity transport equation. This work is reviewed in Coulmy and Luu (1984), where examples of flow past turbine blades are presented. An approach where the vorticity field is discretized by means of vortex carrying particles and velocity is related to vorticity via Biot-Savart integral law was recently proposed for planar problems by Choquin and Huberson (1986).

Vorticity and Stream Function Formulations

In this approach, the continuity equation is written in terms of the stream function, the vorticity transport equation is retained, and velocity is related to the vorticity in the usual way. A hybrid approach was proposed in Wu and Sampath (1976), where an integral equation was used to

represent the continuity condition. Solution was obtained in a transformed domain, with finite differencing used for the vorticity transport equation in conjunction with analytical/numerical treatment of the integral equation. Onishi et al (1985) and Onishi (1986) used standard integral equation representations for the coupled fluid flow-heat conduction system of equations. Heat conduction is described by a parabolic type equation, which is simpler than the vorticity transport equation. The nonlinear and coupling terms were all expressed through volume integrals. The final system of integral equations in both space and time was solved by the boundary element method. The examples solved were two-dimensional and included isothermal channel flow, isothermal flow past a cylinder, and convection-diffusion, wind driven flow in a square cavity. This work was an extension of the authors' work on nonlinear heat transfer problems (Onishi and Kuruki, 1986).

Primitive Variable Formulations

Several recent efforts have focused instead on the more direct velocity-pressure formulation. In particular, Tosaka and Kakuda (1987) developed a primitive variable, incompressible, integral approach by using an approximate time-dependent Stokes fundamental solution. In a second paper, Tosaka (1987) also incorporated thermal effects. However, probably the most important work done on this subject is that of Piva, Graziani and Morino (1987) where they derived the fundamental solution for the linear part of the Navier Stokes equation for incompressible flow.

Compressible Flow

The solution of compressible flow equations is done mostly through finite differences or finite elements. Very little information exists on integral equation based solutions. El-Rafaee et al (1981), for instance,

extended the approach for time dependent incompressible flow of Wu and his co-workers described previously. This was done by adding three transport type equations, one for each of the following dependent variables: dilation, enthalpy, and density. These were coupled with the vorticity transport equation and an augmented integral equation representing the kinematic aspects of flow. A conformal transformation was used to map the region around the airfoil to a regular region outside a circle. An implicit finite difference scheme was used for all the transport equations. The integral equation was numerically evaluated using Fourier series. Problems involving flow over a plate, around a circular cylinder, and around a Joukowski airfoil were solved by this methodology.

Non-Newtonian Fluids

Solutions based on integral equation formulations for non-Newtonian fluids have recently appeared in the literature. In particular, Bush et al (1984) looked at the problem of slow steady extrusion of a jet of Maxwellian fluid. The standard approach of integration by parts was used for the boundary integral equations in terms of the velocity. The non-Newtonian behavior was accounted for through a volume integral of pseudo-body forces exactly as in elasto-plastic analysis of a solid (Banerjee and Butterfield, 1981). The geometry of the axisymmetric problem was discretized via boundary elements and the numerical solution was found to be in good agreement with finite element results. Coleman (1984) approached strong non-Newtonian incompressible flow through a complex variable integral equation formulation for the velocity and stream function. The problem of slow stick-slip flow in a container of finite size was investigated.

Several, perhaps obvious, points should be noted as a conclusion to

this section. First, the set of differential equations governing the behavior of the fluid are much more complicated than those pertaining to the solid. Thus, it is not coincidental that applications of boundary integral techniques for solids has reached a much more refined level, than that for fluids. To the investigators' knowledge, the only integral formulation that has appeared for time-dependent compressible flow is the work done by El Rafaee, Wu and Lekoudis (1981). Even in this work, the vorticity, dilatation, enthalpy, and density transport equations were solved by finite differences. Only the kinematics were represented in integral form. The problems solved were also of simple test problem variety.

Also, it is evident that very little has appeared in the boundary element literature on coupled problems. However, the present investigators have developed a formulation for problems of coupled transient thermoelasticity, which is the subject of the following section.

3. INTEGRAL FORMULATION FOR SOLIDS

3.1 Introduction

In the present section, a surface only time domain boundary element method will be described for a thermoelastic body under quasistatic loading. Thus, transient heat conduction is included, but inertial effects are ignored. Formulations have been developed for three-dimensional, two-dimensional and axisymmetric problems (Dargush, 1987), however, only the 2D plane strain case is detailed below. Separate subsections present the governing differential equations, the integral equations, and an overview of the numerical implementation.

3.2 Governing Equations

With the solid assumed to be a linear thermoelastic medium, the governing differential equations for transient thermoelasticity can be written:

$$(\lambda+\mu)\,\frac{\partial^2 u_j}{\partial x_i \partial x_j} + \mu\,\frac{\partial^2 u_i}{\partial x_j \partial x_j} - (3\lambda+2\mu)\,\alpha\,\frac{\partial \theta}{\partial x_i} = 0 \qquad (3.1a)$$

$$\rho c_\varepsilon\,\frac{\partial \theta}{\partial t} = k\,\frac{\partial^2 \theta}{\partial x_j \partial x_j} \qquad (3.1b)$$

where

u_i	displacement vector
θ	temperature
t	time
x_i	Lagrangian coordinate
k	thermal conductivity
ρ	mass density
c_ε	specific heat at constant deformation

λ, μ Lame's constants

α coefficient of thermal expansion

Standard indicial notation has been employed with summations indicated by repeated indices. For two-dimensional problems considered herein, the Latin indices i and j vary from one to two.

Note that (3.1b) is the energy equation and that (3.1a) represents the momentum balance in terms of displacements and temperature. The theory portrayed by the above set of equations, formally labeled uncoupled quasistatic thermoelasticity, can be derived from thermodynamic principles. (See Boley and Weiner (1960) for details.)

3.3 Integral Representations

Utilizing equation (3.1) for the solid along with a generalized form of the reciprocal theorem, permits one to develop the following boundary integral equation:

$$c_{\beta\alpha}(\xi)u_\beta(\xi,t) = \int_S [\dot{G}_{\beta\alpha} * t_\beta(X,t) - \dot{F}_{\beta\alpha} * u_\beta(X,t)]dS(X) \ . \qquad (3.2)$$

where

α, β indices varying from 1 to 3

s surface of solid

u_α, t_α generalized displacement and traction

$u_\alpha = [u_1 \ u_2 \ \theta]^T$

$t_\alpha = [t_1 \ t_2 \ q]^T$

θ, q temperature, heat flux

$G_{\alpha\beta}, F_{\alpha\beta}$ generalized displacement and traction kernels (Dargush, 1987)

$c_{\alpha\beta}$ constants determined by the relative smoothness of s at ξ

and, for example,

$$\dot{G}_{\alpha\beta} * t_\alpha = \int_0^t \dot{G}_{\alpha\beta}\ (x,t;\ \xi,\tau)\ t_\alpha\ (x,\tau)\ d\tau$$

denotes a Riemann convolution integral.

In principle, at each instant of time progressing from time zero, this equation can be written at every point on the boundary. The collection of the resulting equations could then be solved simultaneously, producing exact values for all the unknown boundary quantities. In reality, of course, discretization is needed to limit this process to a finite number of equations and unknowns. Techniques useful for the discretization of (3.2) are the subject of the following section.

3.4 Numerical Implementation

3.4.1 Introduction

The boundary integral equation (3.2), developed in the last section, is an exact statement. No approximations have been introduced other than those used to formulate the boundary value problem. However, in order to apply (3.2) for the solution of practical engineering problems, approximations are required in both time and space. In this section, an overview of a general-purpose, state-of-the-art numerical implementation is presented. Many of the features and techniques to be discussed, in this section, were developed previously for elastostatics (e.g., Raveendra, 1984) and elastodynamics (e.g., Ahmad, 1986), but are here adapted for thermoelastic analysis.

3.4.2 Temporal Discretization

Consider, first, the time integrals represented in (3.2) as convolutions. Clearly, without any loss of precision, the time interval from zero to t can be divided into N equal increments of duration Δt.

By assuming that the primary field variables, t_β and u_β, are constant

within each Δt time increment, these quantities can be brought outside of the time integral. That is,

$$\dot{G}_{\beta\alpha} * t_\beta(X,t) = \sum_{n=1}^{N} t_\beta^n(X) \int_{(n-1)\Delta t}^{n\Delta t} \dot{G}_{\beta\alpha}(X-\xi, t-\tau)\, d\tau \tag{3.3a}$$

$$\dot{F}_{\beta\alpha} * u_\beta(X,t) = \sum_{n=1}^{N} u_\beta^n(X) \int_{(n-1)\Delta t}^{n\Delta t} \dot{F}_{\beta\alpha}(X-\xi, t-\tau)\, d\tau \ , \tag{3.3b}$$

where the superscript on the generalized tractions and displacements, obviously, represents the time increment number. Notice, also, that, within an increment, these primary field variables are now functions of position only. Next, since the integrands remaining in (3.3) are known in explicit form from the fundamental solutions, the required temporal integration can be performed analytically, and written as

$$G_{\beta\alpha}^{N+1-n}(X-\xi) = \int_{(n-1)\Delta t}^{n\Delta t} \dot{G}_{\beta\alpha}(X-\xi, t-\tau)\, d\tau \tag{3.4a}$$

$$F_{\beta\alpha}^{N+1-n}(X-\xi) = \int_{(n-1)\Delta t}^{n\Delta t} \dot{F}_{\beta\alpha}(X-\xi, t-\tau)\, d\tau \ . \tag{3.4b}$$

These kernel functions, $G_{\beta\alpha}^n(X-\xi)$ and $F_{\beta\alpha}^n(X-\xi)$, are detailed in Appendix B. Combining (3.3) and (3.4) with (3.2) produces

$$c_{\beta\alpha}(\xi) u_\beta^N(\xi) = \sum_{n=1}^{N} \int_S \left[G_{\beta\alpha}^{N+1-n}(X-\xi) t_\beta^n(X) - F_{\beta\alpha}^{N+1-n}(X-\xi) u_\beta^n(X) \right] dS(X) \ , \tag{3.5}$$

which is the boundary integral statement after the application of the temporal discretization.

3.4.3 Spatial Discretization

With the use of generalized primary variables and the incorporation of a piecewise constant time stepping algorithm, the boundary integral equation (3.5) begins to show a strong resemblance to that of elastostatics, particularly for the initial time step (i.e., N=1). In this subsection, those similarities will be exploited to develop the spatial discretization for the coupled quasistatic problem with two-dimensional geometry. This approximate spatial representation will, subsequently, permit numerical evaluation of the surface integrals appearing in (3.5). The techniques described here, actually, originated in the finite element literature, but were later applied to boundary elements by Lachat and Watson (1976).

The process begins by subdividing the entire surface of the body into individual elements of relatively simple shape. The geometry of each element is, then, completely defined by the coordinates of the nodal points and associated interpolation functions. That is,

$$X(\zeta) = x_i(\zeta) = N_w(\zeta)x_{iw} \tag{3.6}$$

with

ζ intrinsic coordinates

N_w shape functions

x_{iw} nodal coordinates

and where w is an integer varying from one to W, the number of geometric nodes in the element. Next, the same type of representation is used, within the element, to describe the primary variables. Thus,

$$u_\alpha^n(\zeta) = N_\omega(\zeta)u_{\alpha\omega}^n \tag{3.7a}$$

$$t_\alpha^n(\zeta) = N_\omega(\zeta)t_{\alpha\omega}^n \tag{3.7b}$$

in which $u^n_{\alpha\omega}$ and $t^n_{\alpha\omega}$ are the nodal values of the generalized displacement and tractions, respectively, for time step n. Also, in (3.7), the integer ω varies from one to Ω, the total number of functional nodes in the element. From the above, note that the same number of nodes, and consequently shape functions, are not necessarily used to describe both the geometric and functional variations. Specifically, in the present work, the geometry is exclusively defined by quadratic shape functions. In two-dimensions, this requires the use of three-noded line elements. On the other hand, the variation of the primary quantities can be described, within an element, by either quadratic or linear shape functions. (The introduction of linear variations proves computationally advantageous in some instances.)

Once this spatial discretization has been accomplished and the body has been subdivided into M elements, the boundary integral equation can be rewritten as

$$c_{\beta\alpha}(\xi)u^N_\beta(\xi) = \sum_{n=1}^{N}\{\sum_{m=1}^{M}\int_{S_m}\Big[\, G^{N+1-n}_{\beta\alpha}(X(\zeta)-\xi)N_\omega(\zeta)t^n_{\beta\omega} - F^{N+1-n}_{\beta\alpha}(X(\zeta)-\xi)N_\omega(\zeta)u^n_{\beta\omega}\,\Big]dS(X(\zeta))\,\}\,, \tag{3.8}$$

where

$$S = \sum_{m=1}^{M}\int S_m\,.$$

In the above equation, $t^n_{\beta\omega}$ and $u^n_{\beta\omega}$ are nodal quantities which can be brought outside the surface integrals. Thus,

$$c_{\beta\alpha}(\xi)u^N_\beta(\xi) = \sum_{n=1}^{N}\{\sum_{m=1}^{M} t^n_{\beta\omega}\int_{S_m} G^{N+1-n}_{\beta\alpha}(X(\zeta)-\xi)N_\omega(\zeta)dS(X(\zeta))$$

$$- u^n_{\beta\omega} \int_{S_m}^{N+1-n} F_{\beta\alpha}(X(\zeta)-\xi)N_\omega(\zeta)dS(X(\zeta)) \quad \} \; . \tag{3.9}$$

The positioning of the nodal primary variables outside the integrals is, of course, a key step, since now the integrands contain only known functions. However, before discussing the techniques used to numerically evaluate these integrals, a brief discussion of the singularities present in the kernels $G^n_{\beta\alpha}$ and $F^n_{\beta\alpha}$ is in order.

The fundamental solutions to the uncoupled quasistatic problem contain singularities when the load point and field point coincide, that is, when $r=0$. The same is true of $G^n_{\beta\alpha}$ and $F^n_{\beta\alpha}$, since these kernels are derived directly from the fundamental solutions. Series expansions of terms present in the evolution functions can be used to deduce the level of singularities existing in the kernels.

A number of observations concerning the results of these expansions should be mentioned. First, as would be expected, $F^1_{\alpha\beta}$ has a stronger level of singularity than does the corresponding $G^1_{\alpha\beta}$, since an additional derivative is involved in obtaining $F^1_{\alpha\beta}$ from $G^1_{\alpha\beta}$. Second, the coupling terms do not have as a high degree of singularity as do the corresponding non-coupling terms. Third, all of the kernel functions for the first time step could actually be rewritten as a sum of steady-state and transient components. That is,

$$G^1_{\alpha\beta} = {}^{ss}G_{\alpha\beta} + {}^{tr}G^1_{\alpha\beta}$$

$$F^1_{\alpha\beta} = {}^{ss}F_{\alpha\beta} + {}^{tr}F^1_{\alpha\beta} \; .$$

Then, the singularity is completely contained in the steady-state portion. Furthermore, the singularity in G^1_{ij} and F^1_{ij} is precisely equal to that for elastostatics, while the $G^1_{\theta\theta}$ and $F^1_{\theta\theta}$ singularities are identical to those

for potential flow. (For two-dimensions, the subscript θ equals three.) This observation is critical in the numerical integration of the $F_{\alpha\beta}$ kernel to be discussed in the next subsection. However, from a physical standpoint, this means simply that, at any time t, the nearer one moves toward the load point, the closer the quasistatic response field corresponds with a steady-state field. Eventually, when the sampling and load points coincide, the quasistatic and steady-state responses are indistinguishable. As a final item, after careful examination of Appendix B, it is evident that the steady-state components in the kernels $G^n_{\alpha\beta}$ and $F^n_{\alpha\beta}$, with $n>1$, vanish. In that case, all that remains is a transient portion that contains no singularities. Thus, all singularities reside in the ${}^{ss}G_{\alpha\beta}$ and ${}^{ss}F_{\alpha\beta}$ components of $G^1_{\alpha\beta}$ and $F^1_{\alpha\beta}$, respectively.

3.4.4 Numerical Integration

Having clarified the potential singularities present in the coupled kernels, it is now possible to consider the evaluation of the integrals in equation (3.9). That is, for any element m, the integrals

$$\int_{S_m} G^{N+1-n}_{\beta\alpha}(X(\zeta)-\xi)N_\omega(\zeta)dS(X(\zeta)) \tag{3.10a}$$

$$\int_{S_m} F^{N+1-n}_{\beta\alpha}(X(\zeta)-\xi)N_\omega(\zeta)dS(X(\zeta)) \tag{3.10b}$$

will be examined. To assist in this endeavor, the following three distinct categories can be identified:

(1) The point ξ does not lie on the element m

(2) The point ξ lies on the element m, but only non-singular or weakly singular integrals are involved

(3) The point ξ lies on the element m, and the integral is strongly singular.

In practical problems involving many elements, it is evident that most of the integration occurring in equation (3.9) will be of the Category (1) variety. In this case, the integrand is always non-singular, and standard Gaussian quadrature formulas can be employed. Sophisticated error control routines are needed, however, to minimize the computational effort for a certain level of accuracy. This non-singular integration is the most expensive part of a boundary element analysis, and, consequently, must be optimized to achieve an efficient solution. In the present implementation, error estimates, based upon the work of Stroud and Secrest (1966), are employed to automatically select the proper order of the quadrature rule. Additionally, to improve accuracy in a cost-effective manner, a graded subdivision of the element is incorporated, especially when ξ is nearby. For two-dimensional problems, the integration order varies from two to twelve, within each of up to four element subdivisions.

Turning next to Category (2), one finds that again Gaussian quadrature is applicable, however, a somewhat modified scheme must be utilized to evaluate the weakly singular integrals. This is accomplished in two-dimensional elements via suitable subsegmentation along the length of the element so that the product of shape function, Jacobian and kernel remains well behaved.

Unfortunately, the remaining strongly singular integrals of Category (3) exist only in the Cauchy principal value sense and cannot, in general, be evaluated numerically, with sufficient precision. It should be noted that this apparent stumbling block is limited to the strongly singular portions, ${}^{ss}F_{ij}$ and ${}^{ss}F_{\theta\theta}$, of the $F^1_{\alpha\beta}$ kernel. The remainder of $F^1_{\alpha\beta}$, including ${}^{tr}F^1_{ij}$ and ${}^{tr}F^1_{\theta\theta}$, can be computed using the procedures outlined for Category (2). However, as will be discussed in the next subsection, even the Category (3) ${}^{ss}F_{ij}$ and ${}^{ss}F_{\theta\theta}$ kernels can be accurately determined

by employing an indirect 'rigid body' method originally developed by Cruse (1974).

3.4.5 Assembly

The complete discretization of the boundary integral equation, in both time and space, has been described, along with the techniques required for numerical integration of the kernels. Now, a system of algebraic equations can be developed to permit the approximate solution of the original quasistatic problem. This is accomplished by systematically writing (3.9) at each global boundary node. The ensuing nodal collocation process, then, produces a global set of equations of the form

$$\sum_{n=1}^{N} \left([G^{N+1-n}]\{t^n\} - [\bar{F}^{N+1-n}]\{u^n\} \right) = \{0\} , \qquad (3.11)$$

where

$[G^{N+1-n}]$ unassembled matrix of size (d+1)P x (d+1)Q, with coefficients determined from (3.10a)

$[\bar{F}^{N+1-n}]$ assembled matrix of size (d+1)P x (d+1)P, with coefficients determined from (3.10b) and $c_{\beta\alpha}$ included in the diagonal blocks

$\{t^n\}$ global generalized nodal traction vector with (d+1)Q components

$\{u^n\}$ global generalized nodal displacement vector with (d+1)P components

$\{0\}$ null vector with (d+1)P components

P total number of global functional nodes

$$Q = \sum_{m=1}^{M} A_m$$

A_m number of functional nodes in element m

d dimensionality of the problem.

In the above, recall that the terms generalized displacement and traction refer to the inclusion of the temperature and flux, respectively, as the (d+1) component at any point.

Consider, now, the first time step. Thus, for N=1, equation (3.11) becomes

$$[G^1]\{t^1\} - [\bar{F}^1]\{u^1\} = \{0\} . \tag{3.12}$$

However, at this point, the diagonal block of $[\bar{F}^1]$ has not been completely determined due to the strongly singular nature of ${}^{ss}F_{ij}$ and ${}^{ss}F_{\theta\theta}$. Following Cruse (1974) and, later, Ahmad (1986) in elastodynamics, these diagonal contributions can be calculated indirectly by imposing a uniform 'rigid body' generalized displacement field on the same body, but under steady-state conditions. Then, obviously, the generalized tractions must be zero, and

$$[{}^{ss}F]\{1\} = \{0\} , \tag{3.13}$$

where {1} is a vector having all (d+1)P components equal to one. Using (3.13), the desired diagonal blocks, ${}^{ss}F_{ij}$ and ${}^{ss}F_{\theta\theta}$, can be obtained from the summation of the off-diagonal terms of $[{}^{ss}F]$. The remaining transient portion of the diagonal block is non-singular, and hence can be evaluated to any desired precision. With that step completed, (3.12) is rewritten as

$$[G^1]\{t^1\} - [F^1]\{u^1\} = \{0\} . \tag{3.14}$$

In a well-posed problem, at time Δt, the set of global generalized nodal displacements and tractions will contain exactly (d+1)P unknown components. Then, as the final stage in the assembly process, equation (3.14) can be rearranged to form

$$[A^1]\{x^1\} = [B^1]\{y^1\} \ , \qquad (3.15)$$

in which

$\{x^1\}$ unknown components of $\{u^1\}$ and $\{t^1\}$

$\{y^1\}$ known components of $\{u^1\}$ and $\{t^1\}$

$[A^1], [B^1]$ associated coefficient matrices.

3.4.6 Solution

To obtain a solution of (3.15) for the unknown nodal quantities, a decomposition of matrix $[A^1]$ is required. In general, $[A^1]$ is a densely populated, unsymmetric matrix. The out-of-core solver, utilized here, was developed originally for elastostatics from the LINPACK software package (Dongarra et al, 1979) and operates on a submatrix level. Within each submatrix, Gaussian elimination with single pivoting reduces the block to upper triangular form. The final decomposed form of $[A^1]$ is stored in a direct-access file for reuse in subsequent time steps. Backsubstitution then completes the determination of $\{x^1\}$. Additional information on this solver is available in Banerjee et al (1985).

After returning from the solver routines, the entire nodal response vectors, $\{u^1\}$ and $\{t^1\}$, at time Δt are known. For solutions at later times, a simple marching algorithm is employed. Thus, from (3.11) with N=2,

$$[G^2]\{t^1\} - [F^2]\{u^1\} + [G^1]\{t^2\} - [F^1]\{u^2\} = \{0\} \ . \qquad (3.16)$$

Assuming that the same set of nodal components are unknown as in (3.14) for the first time step, equation (3.16) is reformulated as

$$[A^1]\{x^2\} = [B^1]\{y^2\} - [G^2]\{t^1\} + [F^2]\{u^1\} \ . \tag{3.17}$$

Since, at this point, the right-hand side contains only known quantities, (3.17) can be solved for $\{x^2\}$. However, the decomposed form of $[A^1]$ already exists on a direct-access file, so only the relatively inexpensive backsubstitution phase is required for the solution.

The generalization of (3.17) to any time step N is simply

$$[A^1]\{x^N\} = [B^1]\{y^N\} - \sum_{n=1}^{N-1} \left([G^{N+1-n}]\{t^n\} - [F^{N+1-n}]\{u^n\} \right) \tag{3.18}$$

in which the summation represents the effect of past events. By systematically storing all of the matrices and nodal response vectors computed during the marching process, surprisingly little computing time is required at each new time step. In fact, for any time step beyond the first, the only major computational task is the integration needed to form $[G^N]$ and $[F^N]$. Even this process is somewhat simplified, since now the kernels are non-singular. Also, as time marches on, the effect of events that occurred during the first time step diminishes. Consequently, the terms containing $[G^N]$ and $[F^N]$ will eventually become insignificant compared to those associated with recent events. Once that point is reached, further integration is unnecessary, and a significant reduction in the computing effort per time step can be achieved.

It should be emphasized that the entire boundary element method developed, in this section, has involved surface quantities exclusively. A complete solution to the well-posed linear coupled quasistatic problem, with homogeneous properties, can be obtained in terms of the nodal response

vectors, without the need for any volume discretization. In many practical situations, however, additional information, such as, the temperature at interior locations or the stress at points on the boundary, is required. The next subsection discusses the calculation of these quantities.

3.4.7 Interior Quantities

Once equation (3.18) is solved, at any time step, the complete set of primary nodal quantities, $\{u^N\}$ and $\{t^N\}$, is known. Subsequently, the response at points within the body can be calculated in a straightforward manner. For any point ξ in the interior, the generalized displacement can be determined from (3.9) with $c_{\beta\alpha} = \delta_{\beta\alpha}$. That is,

$$u^N_\alpha(\xi) = \sum_{n=1}^{N} \{ \sum_{m=1}^{M} [t^n_{\beta\omega} \int_{S_m} G^{N+1-n}_{\beta\alpha}(X(\zeta)-\xi) N_\omega(\zeta) dS(X(\zeta)) - u^n_{\beta\omega} \int_{S_m} F^{N+1-n}_{\beta\alpha}(X(\zeta)-\xi) N_\omega(\zeta) dS(X(\zeta))] \} . \quad (3.19)$$

Now, all the nodal variables on the right-hand side are known, and, as long as, ξ is not on the boundary, the kernel functions in (3.19) remain non-singular. However, when ξ is on the boundary, the strong singularity in $^{ss}F_{\beta\alpha}$ prohibits accurate evaluation of the generalized displacement via (3.19), and an alternate approach is required. The apparent dilemma is easily resolved by recalling that the variation of surface quantities is completely defined by the elemental shape functions. Thus, for boundary points, the desired relationship is simply

$$u^N_\alpha(\xi) = N_\omega(\zeta)\, u^N_{\alpha\omega} \quad (3.20)$$

where $N_\omega(\zeta)$ are the shape functions for the appropriate element and ζ are the intrinsic coordinates corresponding to ξ within that element. Obviously, from (3.20), neither integration nor the explicit contribution

of past events are needed to evaluate generalized boundary displacements.

In many problems, additional quantities, such as heat flux and stress, are also important. The boundary integral equation for heat flux, can be written

$$q_i^N(\xi) = \sum_{n=1}^{N} \{ \sum_{m=1}^{M} [t_{\beta\omega}^n \int_{S_m} E_{\beta\theta i}^{N+1-n}(X(\zeta)-\xi) N_\omega(\zeta) dS(X(\zeta)) - u_{\beta\omega}^n \int_{S_m} D_{\beta\theta i}^{N+1-n}(X(\zeta)-\xi) N_\omega(\zeta) dS(X(\zeta))] \} \tag{3.21}$$

where

$$E_{\beta\theta i}^n(X(\zeta)-\xi) = - k \frac{\partial G_{\beta\theta}^n(X(\zeta)-\xi)}{\partial \xi_i} \tag{3.21a}$$

$$D_{\beta\theta i}^n(X(\zeta)-\xi) = - k \frac{\partial F_{\beta\theta}^n(X(\zeta)-\xi)}{\partial \xi_i} . \tag{3.21b}$$

This is valid for interior points, whereas, when ξ is on the boundary, the shape functions can again be used. In this latter case,

$$N_\omega(\zeta) q_\omega^N = n_i(\xi) q_i^N(\xi) \tag{3.22a}$$

$$\frac{\partial N_\omega(\zeta)}{\partial \zeta} \theta_\omega^N = - \frac{1}{k} \frac{\partial x_i}{\partial \zeta} q_i^N(\xi) , \tag{3.22b}$$

which can be solved for boundary flux. Meanwhile, interior stresses can be evaluated from

$$\sigma_{ij}^N(\xi) = \sum_{n=1}^{N} \{ \sum_{m=1}^{M} [t_{\beta\omega}^n \int_{S_m} E_{\beta ij}^{N+1-n}(X(\zeta)-\xi) N_\omega(\zeta) dS(X(\zeta)) - u_{\beta\omega}^n \int_{S_m} D_{\beta ij}^{N+1-n}(X(\zeta)-\xi) N_\omega(\zeta) dS(X(\zeta))] \} \tag{3.23}$$

in which

$$E^n_{\beta ij}(X(\zeta)-\xi) = \frac{2\mu\nu}{1-2\nu}\,\delta_{ij}\,\frac{\partial G^n_{\beta l}}{\partial \xi_l} + \mu\,\left(\frac{\partial G^n_{\beta i}}{\partial \xi_j} + \frac{\partial G^n_{\beta j}}{\partial \xi_i}\right) - \beta\delta_{ij}G^n_{\beta\theta} \tag{3.23a}$$

$$D^n_{\beta ij}(X(\zeta)-\xi) = \frac{2\mu\nu}{1-2\nu}\,\delta_{ij}\,\frac{\partial F^n_{\beta l}}{\partial \xi_l} + \mu\,\left(\frac{\partial F^n_{\beta i}}{\partial \xi_j} + \frac{\partial F^n_{\beta j}}{\partial \xi_i}\right) - \beta\delta_{ij}F^n_{\beta\theta}\,. \tag{3.23b}$$

Equation (3.23) is, of course, developed from (3.19). Since strong kernel singularities appear when (3.23) is written for boundary points, an alternate procedure is needed to determine surface stress. This alternate scheme exploits the interrelationships between generalized displacement, traction, and stress and is the straightforward extension of the technique typically used in elastostatic implementations. Specifically, the following can be obtained

$$n_j(\xi)\sigma^N_{ij}(\xi) = N_\omega(\zeta)t^N_{i\omega} \tag{3.24a}$$

$$\sigma^N_{ij}(\xi) - \frac{D^e_{ijkl}}{2}\,(u^N_{k,l}(\xi)+u^N_{l,k}(\xi)) = -\,\beta\delta_{ij}N_\omega(\zeta)u^N_{\theta\omega} \tag{3.24b}$$

$$\frac{\partial x_j}{\partial \zeta}\,u^N_{i,j}(\xi) = \frac{\partial N_\omega}{\partial \zeta}\,u^N_{i\omega} \tag{3.24c}$$

in which $u^N_{\theta\omega}$ is obviously the nodal temperatures, and,

$$D^e_{ijkl} = \lambda\delta_{ij}\delta_{kl} + 2\mu\delta_{ik}\delta_{jl}\,.$$

Equations (3.24) form an independent set that can be solved numerically for $\sigma^N_{ij}(\xi)$ and $u^N_{i,j}(\xi)$ completely in terms of known nodal quantities $u^N_{\alpha\omega}$ and $t^N_{\alpha\omega}$, without the need for kernel integration nor convolution. Notice, however, that shape function derivatives appear in (3.24c), thus

constraining the representation of stress on the surface element to something less than full quadratic variation.

The interior stress kernel functions, defined by (3.23), are also detailed in Appendix B.

3.5 Examples of Transient Thermal Stress Analysis

3.5.1 Introduction

The complete plane strain thermoelastic formulation detailed above has been implemented in a general purpose boundary element code. Included are facilities for multiple generic modeling regions (GMR's), sliding or spring interfaces, symmetry, and arbitrary time-dependent boundary conditions.

Several examples are presented in the following subsections to demonstrate the validity and applicability of this boundary-only formulation.

3.5.2 Sudden Heating of an Aluminum Block

As a first example, transient heating of an aluminum block is examined under plane strain conditions. The block, shown in Figure 3.1, initially rests in thermodynamic equilibrium at zero temperature. Then, suddenly, the face at Y = 1.0 in. is elevated to 100^{o}F, while the remaining three faces are insulated and restrained against normal displacements. Thus, only axial deformation in the Y-direction is permitted. Naturally, as the diffusive process progresses, temperature builds along with the lateral stresses σ_{xx} and σ_{zz}. To complete the specification of the problem, the following standard set of material properties are used to characterize the aluminum:

$E = 10 \times 10^{6}$ psi , $\quad \nu = 0.33$,

$\alpha = 13 \times 10^{-6}/^{o}$F ,

$k = 25$ in.-lb./sec. in.^{o}F , $\quad \rho c_{\varepsilon} = 200$ in.-lb./in.^{3o}F .

The two-dimensional boundary element idealization consists of the simple four element, eight node model included in Figure 3.1. A time step of 0.4 sec. is selected, corresponding to a non-dimensional time step of 0.05. Additionally, a finite element analysis of this same problem was conducted using a modified thermal version of the computer code CRISP (Gunn and Britto, 1984). The finite element model is also a two-dimensional plane strain representation, however sixteen linear strain quadralaterals are placed along the diffusion length. In the FE run, a time step of 0.2 sec. is employed.

Temperatures, displacements, and stresses are compared in Table 3.1. Notice that the boundary element analysis, with only one element in the flow direction, produces a better time-temperature history than does a sixteen element FE analysis with a smaller time step. Both methods exhibit greatest error during the initial stages of the process. This is the result of the imposition of a sudden temperature change. Meanwhile, the comparison of the overall axial displacement indicates agreement to within 3% for the BE analysis and 5% for the FE run. A steady-state analysis via both methods produces the exact answer to three digit accuracy. The last comparison, in the table, involves lateral stresses at an integration point in the FE model. The boundary element results are quite good throughout the range, however, the FE stresses exhibit considerable error, particularly during the initial four seconds. Actually, these finite element stress variations are not unexpected in light of the errors present in the temperature and displacement response. Recall that in the standard finite element process, stresses are computed on the basis of numerical differentiation of the displacements, whereas in boundary elements, the stresses at interior points are obtained directly from a discretized version of an exact integral equation. Consequently, the BE interior

stress solution more nearly coincides with the actual response.

3.5.3 Tube and Fin Heat Exchanger

Next, a more realistic problem is examined. The thermal stress distribution, under transient conditions, is often required to evaluate the durability of proposed tube and fin heat exchanger designs. Consider a stainless steel tube with a wall thickness of 0.050in. brazed to a 0.020in. gauge fin of similar material. Figure 3.2 details the geometry. Notice that a fillet radius of 0.015in. is assumed between the tube and fin.

The heat exchanger is cooled continuously by a fluid at $0^{o}F$ flowing inside the tube. It is assumed that this cooling process is of sufficient duration to produce zero temperature, uniformly, throughout the tube and fin. Then, suddenly, at time zero the outer surfaces of the tube and fin are exposed to a $1000^{o}F$ hot gas. The convection coefficients for the inner and outer surfaces are 20 and 10 in.-lb./sec.$in^{2o}F$, respectively. Additionally, the following material properties for the metal apply:

$E = 29x10^{6}$ psi, $\nu = 0.30$,

$\alpha = 9.6x10^{-6}/^{o}F$,

$k = 1.65$ in.-lb./sec.in.^{o}F, $\rho c_{\varepsilon} = 368$ in.-lb./$in.^{3o}F$.

Differences in material behavior near the braze joint are neglected.

For the analysis one-half of a single fin is isolated. The two-dimensional boundary element model is depicted in Figure 3.3. The model consists of two Generic Modeling Regions (GMR's) corresponding roughly to the tube plus braze fillet and the fin. The tube region contains eleven quadratic elements and twenty-two source points, while nine elements and eighteen source points comprise the fin GMR. Some additional interior points are included to enhance the post-processing, however the solution

process remains boundary-only in nature.

The resulting temperature profiles are displayed in Figure 3.4 at 0.25 sec., 0.50 sec., 0.75 sec., and 1.00 sec. The red portions represent temperatures above 750^{o}F, while blue indicates areas below 450^{o}F. As expected, the thin fin, distant from the cold fluid, heats up much more rapidly than the tube. The most severe thermal gradients exist near the braze joint. Von Mises equivalent stresses are plotted in Figure 3.5 for points on the inner tube surface and on the fillet radius. Interestingly, for this particular problem, the transients are not that severe. In fact, the peak transient thermal stresses exceed the steady-state values by only a few percent.

3.5.4 Academic Turbine Blade

For the final thermoelastic example, a two-dimensional slice through an 'academic' turbine blade is examined. The three region boundary element model is shown in Figure 3.6. A total of sixty-four quadratic elements are employed. The blade is assumed to be manufactured from stainless steel with the material properties defined as follows:

$E = 29 \times 10^{6}$ psi, $\nu = 0.30$,

$\alpha = 9.6 \times 10^{-6}/^{o}F$,

$k = 1.65$ in.-lb./sec.in.^{o}F, $\rho c_{\varepsilon} = 368$ in.-lb./in.^{3o}F.

Initially, the entire blade rests unstressed at 0^{o}F, then beginning at time zero all inner and outer surfaces are heated by convection. The gas outside the blade is at 1000^{o}F, while the inner gas temperature is 500^{o}F. The corresponding film coefficients are 2.5 and 3.0 in.-lb./sec.in.^{2o}F, respectively, except at the very tip of the blade where an outer coefficient of 5.0 in.-lb./sec.in.^{2o}F is assumed.

Four temperature profiles during the initial 1.6 sec. of the startup

are depicted in Figure 3.7, in which red represents temperatures above 250°F, yellow 200°F-250°F, green 150°F-200°F, and blue corresponds to temperatures below 150°F. Meanwhile, Figure 3.8 presents the von Mises equivalent stress plot at 0.40 sec. Maximum stresses, greater than 40 ksi, are displayed in red.

Once again, it should be emphasized that this is a boundary-only solution process. No volume discretization is required, and perhaps more importantly, steep through-the-thickness thermal gradients can be accurately captured.

FIGURE 3.1

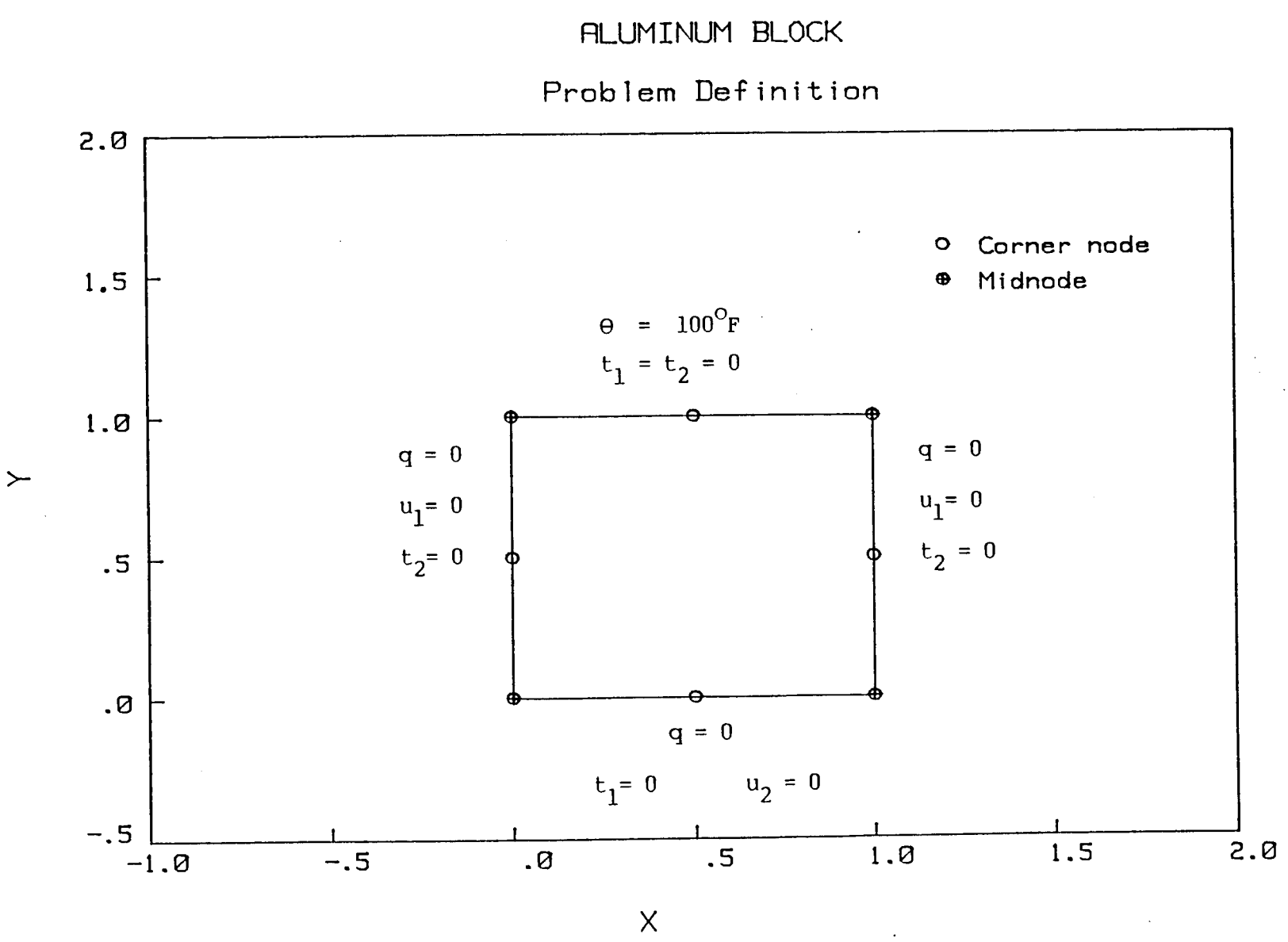
ALUMINUM BLOCK
Problem Definition
Corner node
Midnode
θ = 100°F
t1 = t2 = 0
q = 0
u1 = 0
t2 = 0
q = 0
u1 = 0
t2 = 0
q = 0
t1 = 0
u2 = 0
2.0
1.5
1.0
.5
.0
-.5
-1.0
-.5
.0
.5
1.0
1.5
2.0
Y
X

TABLE 3.1 Sudden Heating of an Aluminum Block

Time (sec)	Temperature (^{o}F) at Y = 0			Axial Displacement (μin.) at Y = 1.0			Lateral Stress (ksi) at Y = 0.5312		
	Exact	FE	BE	Exact	FE	BE	Exact	FE	BE
0.8	4.7	3.4	3.8	910	860	920	-5.6	-3.9	-5.4
1.6	22.0	19.8	20.7	1290	1250	1320	-9.1	-7.7	-9.2
2.4	38.3	36.4	37.7	1570	1540	1610	-11.3	-10.3	-11.7
3.2	51.5	50.0	51.5	1780	1760	1840	-13.1	-12.2	-13.5
4.0	61.9	60.7	62.2	1950	1930	2000	-14.4	-13.8	-14.8
4.8	70.1	69.1	70.5	2090	2070	2130	-15.5	-15.0	-15.9
5.6	76.5	75.7	76.9	2200	2180	2230	-16.3	-15.9	-16.7
6.4	81.5	80.9	81.9	2280	2270	2310	-17.0	-16.7	-17.3
7.2	85.5	84.9	85.8	2340	2330	2370	-17.5	-17.2	-17.8
8.0	88.6	88.2	88.8	2400	2390	2410	-17.9	-17.7	-18.1
∞	100.0	100.0	100.0	2580	2580	2580	-19.4	-19.4	-19.4

FIGURE 3.2

TUBE AND FIN HEAT EXCHANGER

Problem Definition

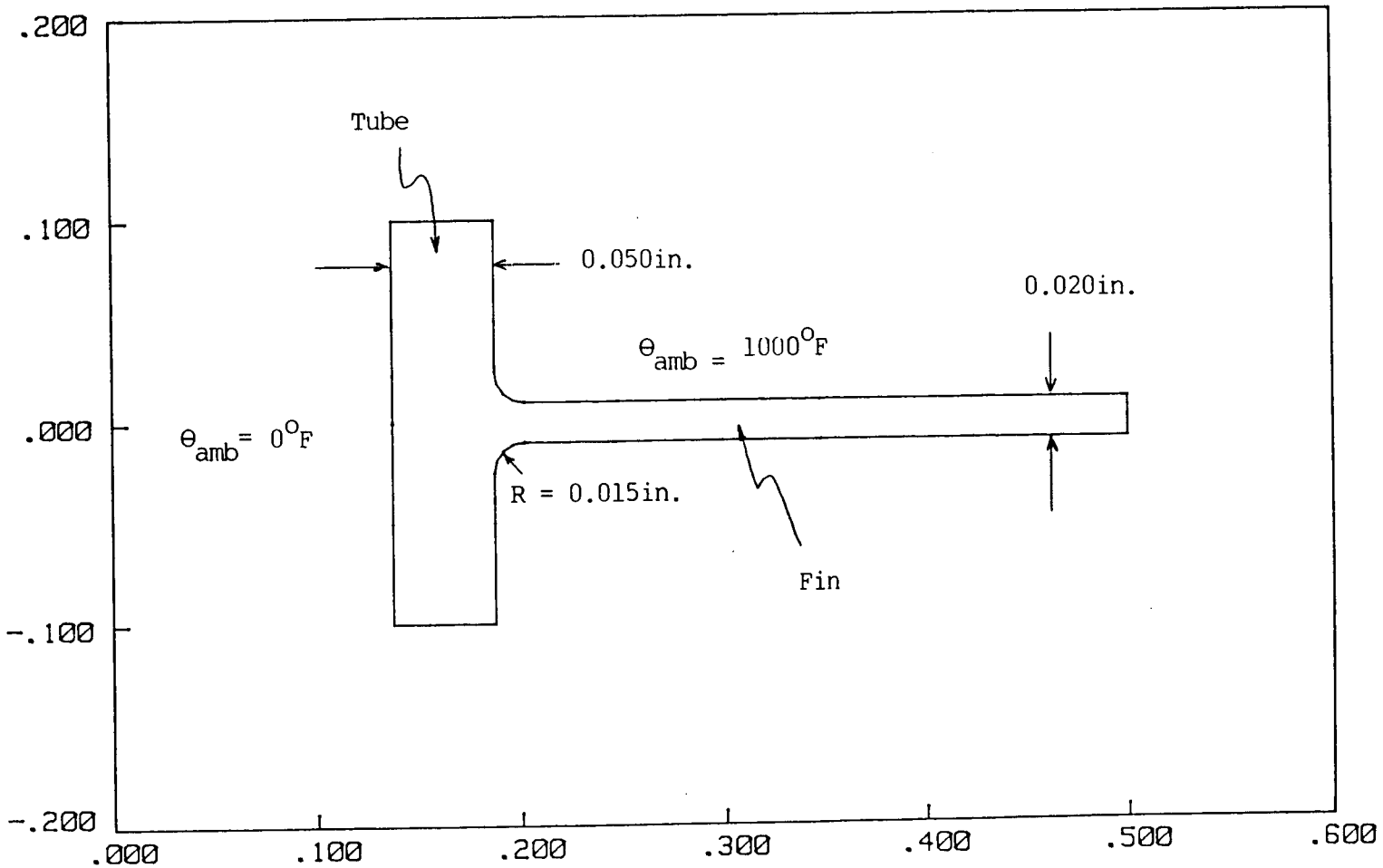

FIGURE 3.3

TUBE AND FIN HEAT EXCHANGER

Boundary Element Model

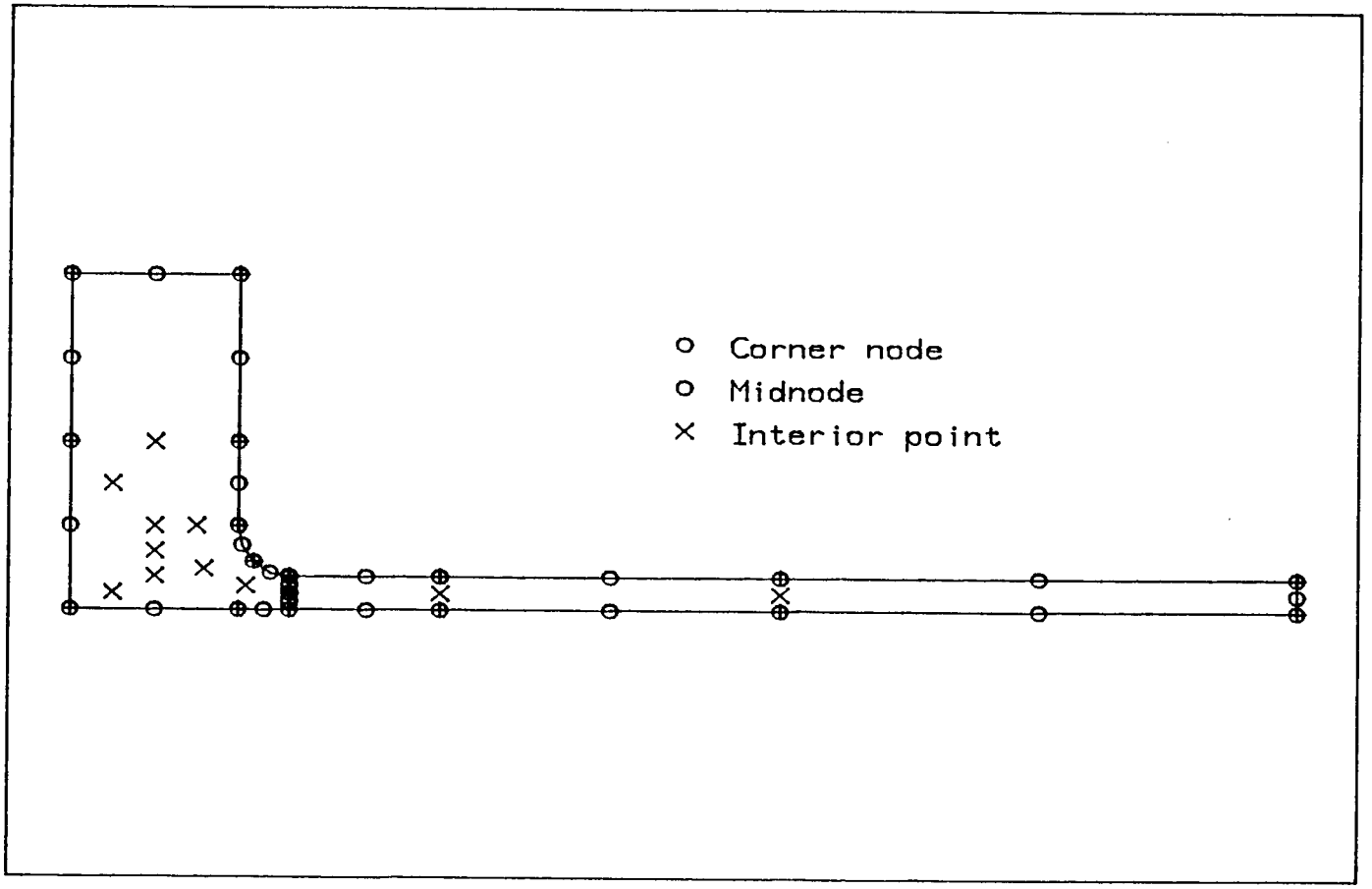

FIGURE 3.4 - TUBE AND FIN HEAT EXCHANGER - TEMPERATURE PROFILES

FIGURE 3.5

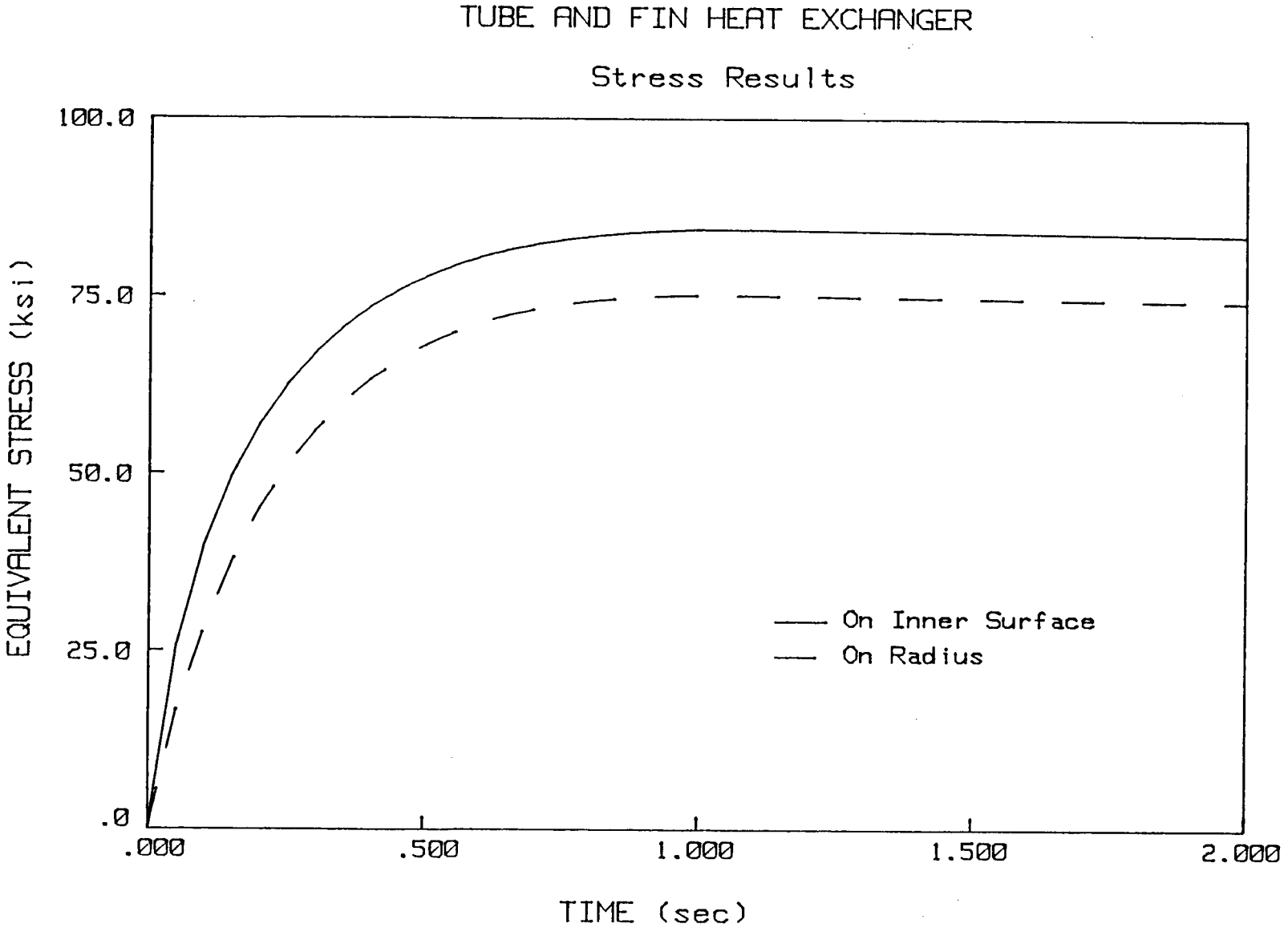
TUBE AND FIN HEAT EXCHANGER
Stress Results
EQUIVALENT STRESS (ksi)
100.0
75.0
50.0
25.0
.0
.000
.500
1.000
1.500
2.000
TIME (sec)
On Inner Surface
On Radius

FIGURE 3.6

ACADEMIC TURBINE BLADE

Boundary Element Model

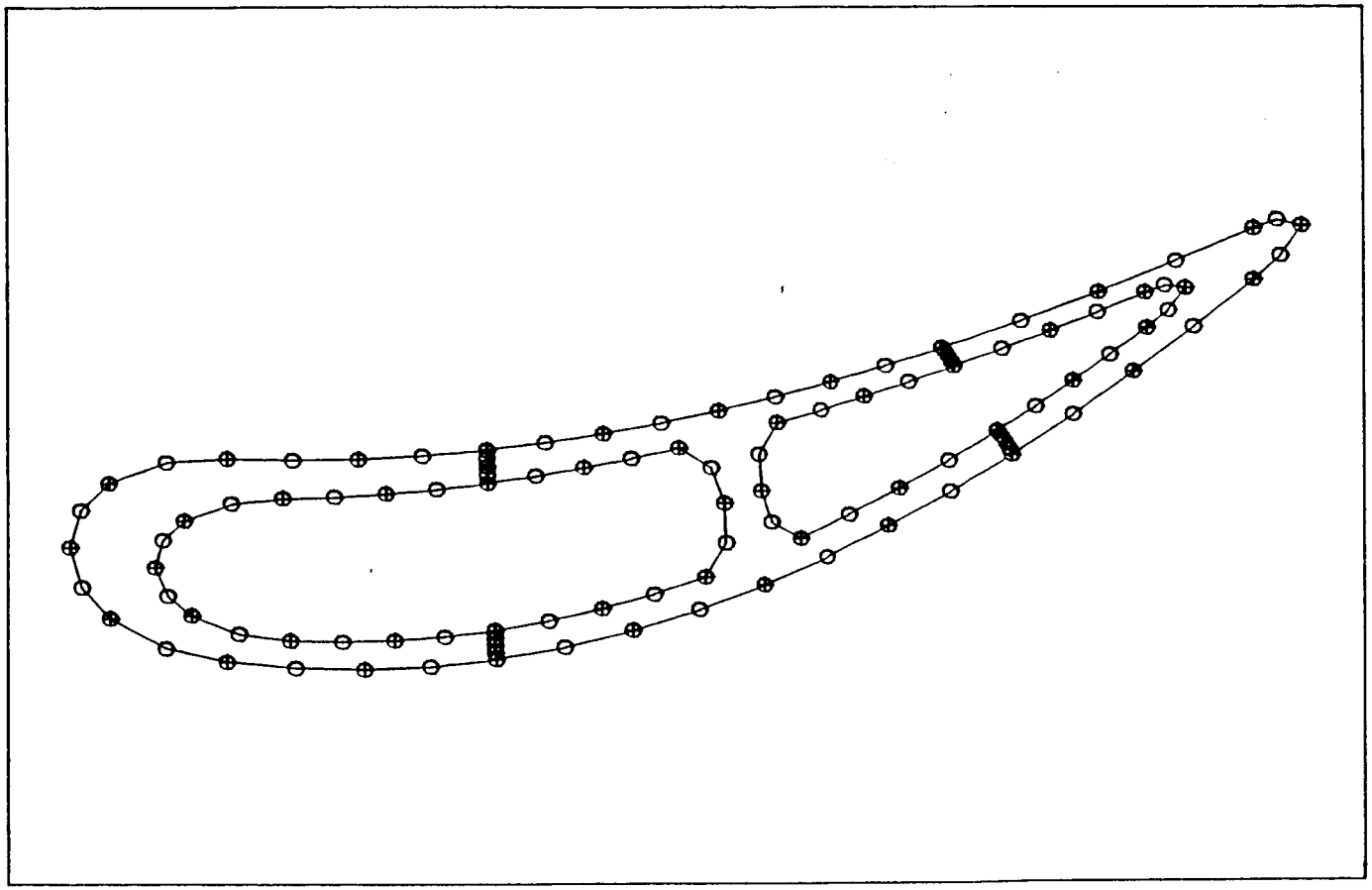

ORIGINAL PAGE
COLOR PHOTOGRAPH

FIGURE 3.7 - ACADEMIC TURBINE BLADE - TEMPERATURE PROFILES

FIGURE 3.8 - ACADEMIC TURBINE BLADE - EQUIVALENT STRESS PROFILE

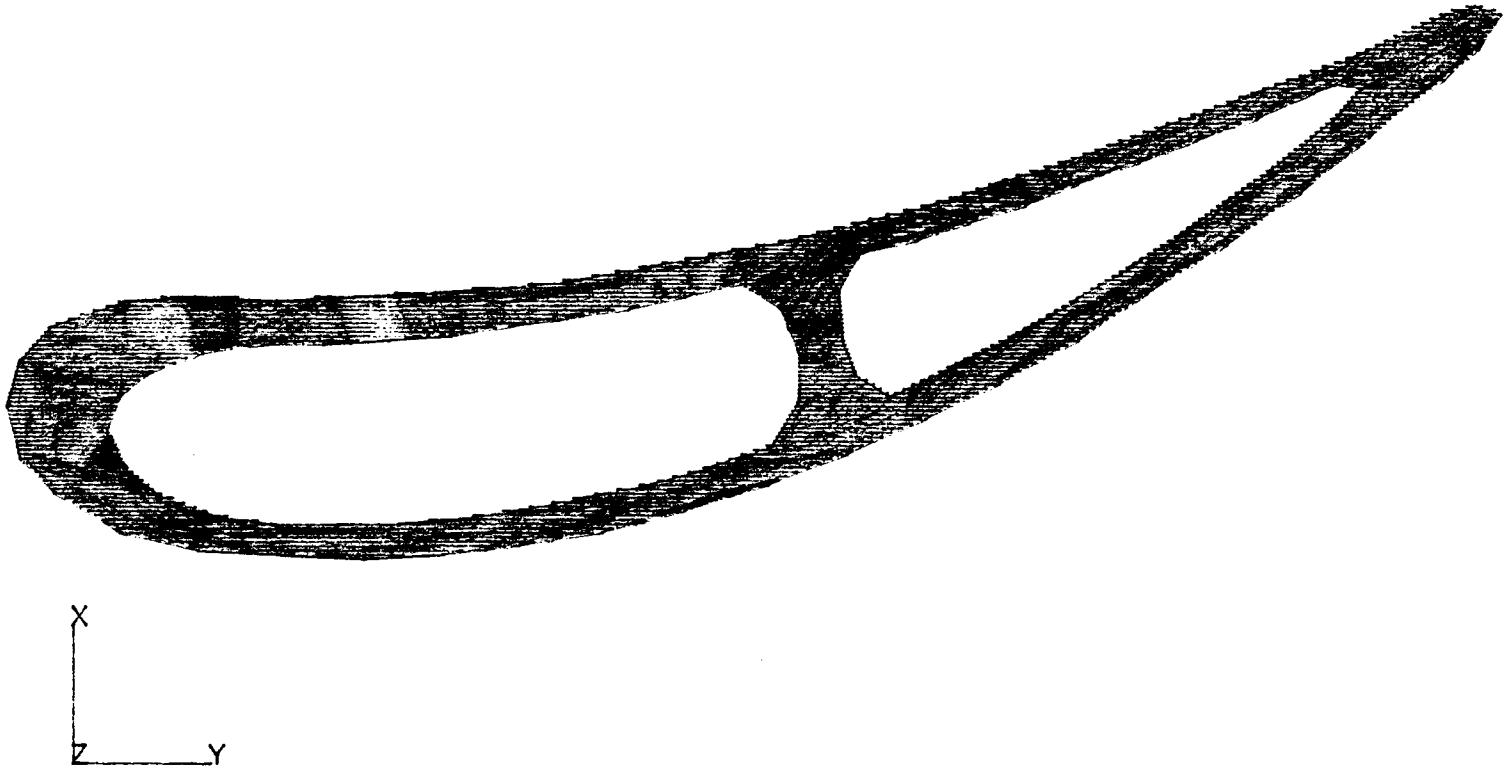

t = 0.4 sec.

ORIGINAL PAGE
COLOR PHOTOGRAPH

4. INTEGRAL FORMULATIONS FOR FLUIDS

4.1 Introduction

Next, attention turns to the hot fluid. In the following, several alternative integral formulations are developed for both incompressible and compressible flow including the effects of thermal coupling. Once again, subsections present the governing equations, the integral equations, and a description of the numerical implementation.

4.2 Governing Differential Equations for Hot Fluid Flow

4.2.1 Time-Dependent Compressible Flow

Initially, the governing equations for a general compressible, Newtonian fluid are presented. This set will provide the basis for the development of the boundary integral representation. (The derivation of these equations can be found in standard fluid mechanics texts. See Yuan (1967), for example.)

The conservation of mass in the absence of sources and sinks in the medium gives the equation of continuity:

$$\frac{\partial \rho}{\partial t} + \frac{\partial (\rho v_i)}{\partial x_i} = 0 \ . \tag{4.1}$$

By introducing kinematics and the constitutive law for a Newtonian fluid with constant coefficients of viscosity, the familiar Navier-Stokes equations appear:

$$\rho \left(\frac{\partial v_i}{\partial t} + v_j \frac{\partial v_i}{\partial x_j}\right) = (\lambda+\mu) \frac{\partial^2 v_j}{\partial x_i \partial x_j} + \mu \frac{\partial^2 v_i}{\partial x_j \partial x_j} - \frac{\partial p}{\partial x_i} \ . \tag{4.2}$$

In the above,

v_i velocity vector

p pressure

t time

x_i Eulerian coordinate

ρ mass density

λ, μ viscosity coefficients.

For a non-Newtonian fluid, additional terms appear in (4.2). However, these terms can be conveniently considered as pseudo-body forces, exactly as done in an elastoplastic analysis of a solid.

Next, the balance expressed by the first law of thermodynamics in conjunction with Fourier's law of heat conduction gives the energy equation as

$$\rho c_v \left(\frac{\partial \theta}{\partial t} + v_i \frac{\partial \theta}{\partial x_i}\right) = k \frac{\partial^2 \theta}{\partial x_i \partial x_i} - p \frac{\partial v_i}{\partial x_i} + Y \qquad (4.3)$$

where, again

θ temperature

k thermal conductivity

and

c_v specific heat at constant volume

Y viscous dissipation.

Note that in (4.3), the thermal conductivity has been assumed constant. Finally, the equation of state for an ideal fluid is introduced to relate temperature and pressure. That is,

$$p = \rho R \theta \qquad (4.4)$$

in which

R gas constant.

The equations (4.1-4.4) represent a coupled set of six equations with six

unknowns, namely v_i, ρ, p and θ. By introducing a characteristic length, velocity, and density, the above equations can be rendered dimensionless. In this case, the familiar Reynolds number (R_e) and Prandtl number (P_r) appear.

Note that these equations have some strong similarities to the governing equations for thermocoupled solids presented in Section 3. This will be exploited in the development of a fluid boundary integral formulation.

4.2.2 Time-Dependent Compressible Flow - Alternative Formulation

The governing differential equations can be recast by introducing the concept of vorticity and dilatation, where vorticity, ω_i, is defined as the curl of the velocity,

$$\omega_i = e_{ijk} \frac{\partial v_k}{\partial x_j} \tag{4.5}$$

and dilatation, e, is the divergence of the velocity,

$$e = \frac{\partial v_j}{\partial x_j} . \tag{4.6}$$

In the above, e_{ijk} is the alternating tensor. Taking the curl of (4.5), the gradient of (4.6), and making use of a vector identity leads to the following relation between velocity, vorticity, and dilatation:

$$\frac{\partial^2 v_i}{\partial x_j \partial x_j} = - e_{ijk} \frac{\partial \omega_k}{\partial x_j} + \frac{\partial e}{\partial x_i} . \tag{4.7}$$

Next, equations (4.2) can be reformulated in terms of vorticity and dilatation. First, taking the curl of (4.2) yields,

$$\rho \left(\frac{\partial \omega_i}{\partial t} + v_j \frac{\partial \omega_i}{\partial x_j}\right) = \mu \frac{\partial^2 \omega_i}{\partial x_j \partial x_j} + \psi_i \ , \tag{4.8}$$

while the divergence of (4.2) produces,

$$\rho \left(\frac{\partial e}{\partial t} + v_j \frac{\partial e}{\partial x_j}\right) = (\lambda+2\mu) \frac{\partial^2 e}{\partial x_j \partial x_j} - \frac{\partial^2 p}{\partial x_j \partial x_j} + \phi \ . \tag{4.9}$$

The functions ψ_i and ϕ in (4.8) and (4.9), respectively, collect additional terms involving v_i, ω_i, e and ρ.

Equations (4.7-4.9) along with (4.1, 4.3 and 4.4) completely define time-dependent compressible flow. While additional equations and unknowns appear in this alternative formulation, there are also some advantages. Most importantly, the kinematics and the kinetics of the problem are separated, with (4.7) expressing the kinematics and (4.8) and (4.9) the kinetics. The kinetic equations need only be considered in regions of nonvanishing vorticity, for the case of (4.8), and nonzero dilatation, for (4.9). Since, in general, the vortical region will be confined to a small portion of the entire fluid domain, significant reduction in computational effort is possible. Additionally, it should be noted that the equations take on a somewhat simplified and unified form. Equation (4.7) is a vector form of Poisson's equation for v_i, while (4.8), (4.9), and (4.3) are all of a similar nature, representing the transport of vorticity, dilatation, and temperature, respectively.

4.2.3 Time-Dependent Incompressible Flow

For incompressibility, ρ is constant and the continuity condition becomes simply

$$\frac{\partial v_i}{\partial x_i} = 0, \tag{4.10}$$

while the equations of motion reduce to

$$\rho \left(\frac{\partial v_i}{\partial t} + v_j \frac{\partial v_i}{\partial x_j}\right) = \mu \frac{\partial^2 v_i}{\partial x_j \partial x_j} - \frac{\partial p}{\partial x_i} \,. \tag{4.11}$$

For three-dimensional problems, (4.10) and (4.11) form a system of four equations in the unknowns v_i and p. The equations of energy and state are no longer required to determine fluid motion. However, under non-isothermal conditions, the fluid temperatures can be obtained from (4.3) after the velocities are established. The exception, to this two stage approach, is for buoyancy driven flow in which the body forces produced by temperature gradients are dominant. In this latter case, continuity (4.10), momentum (4.11) and energy (4.3) conservation must be satisfied simultaneously.

4.2.4 Time-Dependent Incompressible Flow - Alternative Formulation

For the case of incompressible flow, the dilatation is everywhere zero and the formulation of Section 4.2.2 simplifies. The kinematics reduce to

$$\frac{\partial^2 v_i}{\partial x_j \partial x_j} = - e_{ijk} \frac{\partial \omega_k}{\partial x_j} \tag{4.12}$$

and the kinetics are completely defined by the vorticity transport equation

$$\rho \left(\frac{\partial \omega_i}{\partial t} + v_j \frac{\partial \omega_i}{\partial x_j} - \omega_j \frac{\partial v_i}{\partial x_j}\right) = \mu \frac{\partial^2 \omega_i}{\partial x_j \partial x_j} \,. \tag{4.13}$$

Now there is a system of six equations in six unknowns, v_i and ω_i. Again, this approach has the advantage that the kinematic and kinetic aspects of flow are separated. It has been used by a number of BEM researchers (Wu and Thompson (1973), Coulmy (1976)) for a number of simple test problems in

two-dimensions, where the vorticity becomes a scalar.

4.3 Integral Representations

4.3.1 Introduction

Although in the previous section, complete sets of governing differential equations for various forms of fluid flow are described, from the practical point of view, only the velocity, pressure and temperature form will be sufficiently general. During the early stages of the present work (1986-87), the vorticity formulation was implemented. It was observed that while this formulation has some very convenient features, incorporation of appropriate boundary conditions for a practical problem becomes a difficult task. At the later stages of the current work, it may be possible to incorporate these vorticity integrals within a coupled compressible potential flow - convective heat transfer formulation to provide a very cost effective method for the solution of the present problem. Before such an approximate method can be developed, it is important to examine the full scale implementation of the complete governing equations without any approximation.

4.3.2 Fundamental Solution

It is convenient to rewrite the governing differential equations (4.1-4.4) for the velocity - pressure - temperature formulation of compressible viscous flow as follows:

$$(\lambda+\mu)\frac{\partial^2 v_j}{\partial x_i \partial x_j} + \mu\frac{\partial^2 v_i}{\partial x_j \partial x_j} + f_i' - \rho_r R\frac{\partial \theta}{\partial x_i} - \rho_r\frac{\partial v_i}{\partial t} = 0 \qquad (4.14a)$$

$$k\frac{\partial^2 \theta}{\partial x_j \partial x_j} - \rho_r c_v\frac{\partial \theta}{\partial t} + \psi = 0 \qquad (4.14b)$$

where

$$f_i' = -\rho_v \frac{\partial v_i}{\partial t} - \rho v_j \frac{\partial v_i}{\partial x_j} - \rho_v R \frac{\partial \theta}{\partial x_i} - R\theta \frac{\partial \rho}{\partial x_i}$$

$$\psi = -\rho_v c_v \frac{\partial \theta}{\partial t} - \rho c_v v_j \frac{\partial \theta}{\partial x_j} - \rho R\theta \frac{\partial v_j}{\partial x_j} + Y$$

$$Y = \left[\mu \left(\frac{\partial v_i}{\partial x_j} + \frac{\partial v_j}{\partial x_i} \right) + \lambda \delta_{ij} \frac{\partial v_k}{\partial x_k} \right] \frac{\partial v_i}{\partial x_j} = \sigma_{ij}^{*} \frac{\partial v_i}{\partial x_j}$$

$\rho = \rho_r + \rho_v$

ρ_r reference density

ρ_v variable density

$$\frac{\partial \rho}{\partial t} + v_j \frac{\partial \rho}{\partial x_j} + \rho \frac{\partial v_j}{\partial x_j} = 0$$

$p = \rho R\theta$

One of the primary requirements of developing a boundary element formulation is that the fundamental solution of the governing differential equation (4.14) must exist. These fundamental solutions can be viewed in same sense as the shape functions in the finite element method. For solid mechanics these have been very well explored. Starting with Kelvin's solution (1846), investigators such as Stokes, Poisson, Boussinesq, Mindlin, and Nowacki have provided both static and transient solutions which form the basis of the boundary element formulations in solid mechanics. It is unfortunate that workers in fluid mechanics have not found any use for these fundamental solutions in the infinite space and therefore have not made any attempt to derive such solutions. Since the boundary element formulations could not be developed without these

solutions, a substantial amount of effort was devoted in the present work to successively derive more and more complete solutions of the differential equations (4.14). As a first approximation the compressibility terms in (4.14) were ignored and the complete fundamental solution for a transient body force and a transient heat source was derived as presented below. In a subsequent effort these were extended to include the effect of compressibility, which of course, reduces the elegance of some of these solutions and therefore is not reproduced here. It should be noted that the time dependent incompressible solution given here can also be used for compressible flow because the body force can be adjusted to allow for the effects of compressibility (i.e., terms involving ρ_v in (4.14)). The solution presented below is developed for the three-dimensional space. The corresponding two-dimensional case can be shown to formally follow the same procedure.

The governing differential equation for an incompressible, viscous fluid can be written as:

$$(\lambda+\mu)\frac{\partial^2 v_j}{\partial x_i \partial x_j} + \mu \frac{\partial^2 v_i}{\partial x_j \partial_j} - \frac{\partial p}{\partial x_i} - \rho \frac{\partial v_i}{\partial t} + f_i = 0 \qquad (4.15a)$$

$$\frac{\partial v_j}{\partial x_j} = 0 \ . \qquad (4.15b)$$

Via the well-known Helmholtz decomposition the vectors v_i and f_i become

$$v_i = v_{,i} + e_{ijk} V_{k,j} \qquad (4.16a)$$

$$f_i = f_{,i} + e_{ijk} F_{k,j} \qquad (4.16b)$$

with $V_{i,i} = 0$ and $F_{i,i} = 0$ for definiteness. Then, equations (4.15) become

$$(\lambda+\mu)\left[\frac{\partial^2(v_{,j}+e_{jlm}V_{m,l})}{\partial x_i \partial x_j}\right] + \mu\left[\frac{\partial^2(v_{,l}+e_{ilm}V_{m,l})}{\partial x_j \partial x_j}\right] - \frac{\partial p}{\partial x_i}$$

$$- \rho\left[\frac{\partial(v_{,l}+e_{ilm}V_{m,l})}{\partial t}\right] + f_{,i} + e_{ilm}F_{m,l} = 0 \qquad (4.17a)$$

$$\frac{\partial(v_{,ij}+e_{jlm}V_{m,l})}{\partial x_j} = 0 \ . \qquad (4.17b)$$

But, since

$$\frac{\partial(e_{jlm}A_{m,l})}{\partial x_j} = 0 \ ,$$

equations (4.17) reduce to

$$(\lambda+\mu)\left[\frac{\partial}{\partial x_i}(v_{,jj})\right] + \mu\left[\frac{\partial}{\partial x_i}(v_{,jj}) + e_{ilm}\frac{\partial}{\partial x_l}(V_{m,jj})\right] - \frac{\partial p}{\partial x_i}$$

$$- \rho\left[\frac{\partial}{\partial x_i}\left(\frac{\partial v}{\partial t}\right) + e_{ilm}\frac{\partial}{\partial x_i}\left(\frac{\partial V_m}{\partial t}\right)\right] + \frac{\partial f}{\partial x_i} + e_{ilm}\frac{\partial F_m}{\partial x_i} = 0 \qquad (4.18a)$$

$$v_{,jj} = 0 \ . \qquad (4.18b)$$

Grouping terms, equation (4.18a) becomes

$$\frac{\partial}{\partial x_i}\left[(\lambda+\mu)\, v_{,jj} + \mu v_{,jj} - p - \rho\frac{\partial v}{\partial t} + f\right]$$

$$+ e_{ilm}\frac{\partial}{\partial x_i}\left[\mu V_{m,jj} - \rho\frac{\partial V_m}{\partial t} + F_m\right] = 0 \ . \qquad (4.19)$$

For generality, the bracketed terms must vanish independently. Thus,

$$(\lambda+2\mu)v_{,jj} - \rho\frac{\partial v}{\partial t} - p+f = 0 \qquad (4.20a)$$

$$\mu V_{m,jj} - \rho\frac{\partial V_m}{\partial t} + F_m = 0 \ . \qquad (4.20b)$$

However, after enforcing (4.18b), these become

$$- \rho \frac{\partial v}{\partial t} - p+f = 0 \tag{4.21a}$$

$$\mu V_{m,jj} = \rho \frac{\partial V_m}{\partial t} + F_m = 0 \ . \tag{4.21b}$$

Next, a unit pulse force in the i-direction applied at point $\bar{x}_o$ and time t_o must be decomposed. That is, let

$$f_i = \delta(\bar{x}-\bar{x}_o)\delta(t-t_o)e_i .$$

From the properties of the delta function in three dimensional space, this can be rewritten as

$$f_i = - \frac{\delta(t-t_o)}{4\pi} \left(\frac{e_i}{r}\right)_{,jj}$$

in which

$$y_i = x_i - x_{io}$$

$$r^2 = y_i y_i \ .$$

But noting

$$A_{i,jj} = A_{j,ij} - e_{ijk}e_{klm}A_{m,lj}$$

thus,

$$f_i = - \frac{\delta(t-t_o)}{4\pi} \left[\left(\frac{e_j}{r}\right)_{,ij} - e_{ijk}e_{klm} \left(\frac{e_m}{r}\right)_{,lj} \right] .$$

Then, from (4.16b), the decomposition of f_i can be written

$$f = - \frac{\delta(t-t_o)}{4\pi} e_j \left(\frac{1}{r}\right)_{,j} \tag{4.22a}$$

$$F_k = e_{klm} \frac{\delta(t-t_o)e_m}{4\pi} \left(\frac{1}{r}\right)_{,l} . \tag{4.22b}$$

Substituting (4.22) into (4.21) yields

$$-\rho \frac{\partial v}{\partial t} - p - \frac{\delta(t-t_o)e_j}{4\pi} \left(\frac{1}{r}\right)_{,j} = 0 \tag{4.23a}$$

$$\mu V_{m,ll} - \rho \frac{\partial V_m}{\partial t} + e_{mlk} \frac{\delta(t-t_o)e_k}{4\pi} \left(\frac{1}{r}\right)_{,l} = 0 . \tag{4.23b}$$

The fundamental point force solution is any particular solution which satisfies (4.23) along with the incompressibility constraint,

$$v_{,jj} = 0 . \tag{4.18b}$$

First, let the scalar function, v, be identically zero. That is, let $v(\bar{x},t;\bar{x}_o t_o) = 0$. This obviously satisfies (4.18b), and permits the reduction of (4.23a) to simply

$$p = -\frac{\delta(t-t_o)e_j}{4\pi} \left(\frac{1}{r}\right)_{,j} .$$

Carrying out the differentiation, this can be rewritten as

$$p(\bar{x},t;\bar{x}_o,t_o) = \frac{\delta(t-t_o)e_j}{4\pi r^2} \left(\frac{y_j}{r}\right) . \tag{4.24}$$

Thus, (4.24) satisfies (4.18b) and (4.23a). All that remains is to find a solution, $V_m(\bar{x},t)$, of equation (4.23b). With that in mind, a Helmholtz decomposition can again be applied. That is, let

$$V_m = u_{,m} + e_{mij}U_{j,i} \tag{4.25}$$

with $U_{i,i} = 0$ for definiteness. Substituting (4.25) into (4.23b) produces

$$\mu \left[u_{,mll} + e_{mij} U_{j,ill} \right] - \rho \left[\frac{\partial u_{,m}}{\partial t} + e_{mij} \frac{\partial U_{j,i}}{\partial t} \right]$$

$$+ e_{mlk} \frac{\delta(t-t_o)e_k}{4\pi} \left(\frac{1}{r}\right)_{,l} = 0 \ ,$$

or after some rearrangement

$$\frac{\partial}{\partial x_m} \left[\mu u_{,ll} - \rho \frac{\partial u}{\partial t} \right] + e_{mij} \frac{\partial}{\partial x_i} \left[\mu U_{j,ll} - \rho \frac{\partial U_j}{\partial t} + \frac{\delta(t-t_o)e_j}{4\pi r} \right] = 0 \ . \tag{4.26}$$

For generality, both bracketed expressions must vanish independently. However, since from (4.16a), $V_{m,m} = 0$, it follows that u must satisfy

$$u_{,ii} = 0$$

and consequently ,

$$\frac{\partial u}{\partial t} = 0 \ .$$

Thus, let u = 0. From the second set of bracketed terms in (4.26),

$$\mu U_{j,ll} - \rho \frac{\partial U_j}{\partial t} + \frac{\delta(t-t_o)e_j}{4\pi r} = 0.$$

This is simply a vector version of the diffusion equation. After letting $U_j = Ue_j$, this can be rewritten in the form of the standard scalar diffusion equation as

$$cU_{,ii} - \frac{\partial U}{\partial t} + \psi = 0 \tag{4.27}$$

in which

$$c = \frac{\mu}{\rho}$$

$$\psi = \frac{\delta(t-t_o)}{4\pi\rho r} .$$

A particular solution of (4.27) can then be obtained by utilizing a Green's function approach for the diffusion equation on an infinite domain with sources ψ and zero initial conditions. Therefore,

$$U(\bar{x},t;\bar{x}_o,t_o) = \int_{V_\infty} \dot{G}(\bar{x},t;\bar{z},\tau)*\psi(\bar{z},\tau;\bar{x}_o,t_o)dV(\bar{z}) \tag{4.28}$$

where

$$\dot{G}(\bar{x},t;\bar{z},\tau) = \frac{e^{-\eta^2/4}}{[4\pi c(t-\tau)]^{3/2}} \tag{4.29}$$

is the infinite space point pulse source Green's function with

$$\eta^2 = \frac{\gamma^2}{c(t-\tau)}$$

$$\gamma = |\bar{x} - \bar{z}| .$$

Furthermore, the volume integration in (4.28) is conducted over the infinite space V_∞ and the operator $*$ represents a Riemann convolution integral defined by

$$g(t)*h(t) = \int_0^t g(t-\tau)h(\tau)d\tau = \int_0^t g(\tau)h(t-\tau)d\tau .$$

Now, also define

$$\varepsilon = |\bar{z} - \bar{x}_o| ,$$

so that the source term can be rewritten as

$$\psi(\bar{z},\tau;\bar{x}_o,t_o) = \frac{\delta(\tau-t_o)}{4\pi\rho\varepsilon} .$$

Thus,

$$\dot{G}^{*}\psi = \int_0^t \frac{e^{-\eta^2/4}}{[4\pi c(t-\tau)]^{3/2}} \frac{\delta(\tau-t_o)}{4\pi\rho\varepsilon} d\tau = \frac{H(t-t_o)}{4\pi\rho\varepsilon} \frac{e^{-\gamma^2/4c(t-t_o)}}{[4\pi c(t-t_o)]^{3/2}} \qquad (4.30)$$

with a redefinition of η as

$$\eta^2 = \frac{\gamma^2}{c(t-t_o)} .$$

Then, the substitution of (4.30) into (4.28) yields

$$U(\bar{x},t;\bar{x}_o,t_o) = \int_{V_\infty} \frac{H(t-t_o)}{4\pi\rho\varepsilon} \frac{e^{-\eta^2/4}}{[4\pi c(t-t_o)]^{3/2}} dV(\bar{z}) . \qquad (4.31)$$

To carry out this volume integration, a spherical coordinate system can be constructed with the point $\bar{x}_o$ at the origin, as shown in Figure 4.1.

Then equation (4.31) becomes

$$U(\bar{x},t;\bar{x}_o,t_o) = \int_0^\infty \int_0^\pi \int_0^{2\pi} \frac{H(t-t_o)}{4\pi\rho\varepsilon} \frac{e^{-\eta^2/4}}{[4\pi c(t-t_o)]^{3/2}} \varepsilon^2 \sin\phi d\varepsilon d\phi d\theta$$

$$= \frac{2\pi}{(4\pi)^{5/2}} \frac{H(t-t_o)}{\rho[c(t-t_o)]^{3/2}} \int_0^\infty \int_0^\pi \varepsilon e^{-\eta^2/4} \sin\phi d\varepsilon d\theta .$$

But,

$$\eta = \frac{\gamma}{[c(t-t_o)]^{1/2}} = \left(\frac{\varepsilon^2+r^2-2\varepsilon r\cos\phi}{c(t-t_o)}\right)^{1/2}$$

$$\frac{d\eta}{d\phi} = \frac{1}{2} \left(\frac{\varepsilon^2+r^2-2\eta r\cos\phi}{c(t-t_o)}\right)^{1/2} \left(\frac{2\varepsilon r\sin\phi}{c(t-t_o)}\right) = \frac{r}{c(t-t_o)} \frac{\varepsilon}{\eta} \sin\phi .$$

Thus,

$$U(\bar{x},t;\bar{x}_o,t_o) = \frac{H(t-t_o)c(t-t_o)}{2\rho r[4\pi c(t-t_o)]^{3/2}} \int_0^\infty \int_{\eta_o}^{\eta_\pi} \eta e^{-\eta^2/4} d\eta d\varepsilon$$

where

$$\eta_o = \left(\frac{\varepsilon^2+r^2-2\varepsilon r}{c(t-t_o)}\right)^{1/2}$$

$$\eta_\pi = \left(\frac{\varepsilon^2+r^2+2\varepsilon r}{c(t-t_o)}\right)^{1/2} .$$

Next, using the substitution

$$s = \frac{\eta^2}{4} ,$$

the integral over η becomes

$$\int_{\eta_o}^{\eta_\pi} \eta e^{-\eta^2/4}\, d\eta = \int_{u_o}^{u_\pi} 2e^{-u} du = -2e^{-u}\Big|_{u_o}^{u_\pi} = -2e^{-\frac{(\varepsilon+r)^2}{4c(t-t_o)}} + 2e^{-\frac{(\varepsilon-r)^2}{4c(t-t_o)}}.$$

Consequently,

$$U(\bar{x},t;\bar{x}_o,t_o) = -\frac{H(t-t_o)c(t-t_o)}{[4\pi c(t-t_o)]^{3/2}}\left(\frac{1}{\rho r}\right)\left[\int_0^\infty e^{-\frac{(\varepsilon+r)^2}{4c(t-t_o)}} d\varepsilon - \int_0^\infty e^{-\frac{(\varepsilon-r)^2}{4c(t-t_o)}} d\varepsilon\right].$$

Now, make use of the substitutions

$$w = \frac{\varepsilon+r}{[4c(t-t_o]^{1/2}}$$

$$y = \frac{\varepsilon-r}{[4c(t-t_o]^{1/2}} ,$$

and rewrite the ε integrals as

$$\int_0^\infty e^{-\frac{(\varepsilon+r)^2}{4c(t-t_o)}} d\varepsilon = [4c(t-t_o)]^{1/2} \int_{\frac{r}{[4c(t-t_o)]^{1/2}}}^\infty e^{-w^2} dw$$

$$= [4c(t-t_o)]^{1/2} \frac{\sqrt{\pi}}{2} \operatorname{erfc}\left(\frac{r}{[4c(t-t_o)]^{1/2}}\right)$$

$$\int_0^\infty e^{-\frac{(\varepsilon-r)^2}{4c(t-t_o)}} d\varepsilon = [4c(t-t_o)]^{1/2} \int_{\frac{r}{[4c(t-t_o)]^{1/2}}}^{\infty} e^{-y^2} dy$$

$$= [4c(t-t_o)]^{1/2} \frac{\sqrt{\pi}}{2} \operatorname{erfc}\left(\frac{-r}{[4c(t-t_o)]^{1/2}}\right) .$$

Thus,

$$U(\bar{x},t;\bar{x}_o t_o) = - \frac{H(t-t_o)}{8\pi\rho r} \left[\operatorname{erfc}\left(\frac{r}{[4c(t-t_o)]^{1/2}}\right) - \operatorname{erfc}\left(\frac{-r}{[4c(t-t_o)]^{1/2}}\right) \right] , \tag{4.32}$$

but, since

$$\operatorname{erfc}(z) = 1 - \operatorname{erf}(z)$$

$$\operatorname{erf}(-z) = - \operatorname{erf}(z)$$

equation (4.32) simplifies to

$$U(\bar{x},t;\bar{x}_o,t_o) = \frac{H(t-t_o)}{4\pi\rho r} \operatorname{erf}\left(\frac{r}{\sqrt{4c(t-t_o)}}\right) . \tag{4.33}$$

With the function U now established, the fundamental solution can be reconstructed. From (4.16a) and (4.25),

$$v_i = v_{,i} + e_{ijk} u_{,kj} + e_{ijk} e_{klm} U_{m,lj} .$$

However, since both v and u are identically zero, this reduces to

$$v_i = e_{ijk} e_{klm} U_{m,lj} ,$$

which can be rewritten as

$$v_i = U_{j,ij} - U_{i,jj} = U_{,ij}e_j - U_{,jj}e_i$$

or, for a unit pulse point force in the j-direction,

$$v_i(\bar{x},t;\bar{x}_o,t_o) = (U_{,ij} - \delta_{ij}U_{,kk})e_j \ .$$

Therefore, the desired fundamental solution becomes

$$\dot{G}_{ij}(\bar{x},t;\bar{x}_o,t_o) = U_{,ij} - \delta_{ij}U_{,kk} \tag{4.34a}$$

$$\dot{P}_j(\bar{x},t;\bar{x}_o,t_o) = \frac{\delta(t-t_o)}{4\pi r^2}\left(\frac{y_j}{r}\right) \tag{4.34b}$$

with

$$U = \frac{H(t-t_o)}{4\pi\rho r}\ \mathrm{erf}\ \left(\frac{r}{\sqrt{4c(t-t_o)}}\right) \tag{4.34c}$$

in which $\dot{G}_{ij}$ is the velocity in the i-direction and $\dot{P}_j$ is the pressure, due to a unit pulse point force in the j-direction.

As a first approximation, this can be combined, along with the standard diffusive unit pulse heat source solution to produce a boundary integral formulation for non-isothermal incompressible flow. In the compressible case, a reference density is introduced, as shown in (4.14). Furthermore, a dilatational component apears in $\dot{G}_{ij}$, along with thermal coupling terms. The investigators are currently developing the required fundamental solutions for the set of differential equations (4.14). Most of the algebraic work is completed. Some tidying up of the final solution is in progress.

4.3.3 Reciprocal Theorem

For any two unrelated states of body forces, surface tractions, velocities and temperatures $(f_i^{(1)}, t_i^{(1)}, v_i^{(1)}, \theta^{(1)})$ and

$(f_i^{(2)}, t_i^{(2)} v_i^{(2)}, \theta^{(2)})$ existing in the same region v bounded by the surface s, the following reciprocal integral identity holds:

$$\int_s \left[\dot{t}_i^{(1)} * v_i^{(2)} + q^{(1)} * \theta^{(2)} - \dot{v}_i^{(1)} * t_i'^{(2)} - \theta^{(1)} * q^{(2)} \right] dS$$

$$+ \int_v \left[\dot{f}_i^{(1)} * v_i^{(2)} + \psi^{(1)} * \theta^{(2)} - \dot{v}_i^{(1)} * f_i'^{(2)} - \theta^{(1)} * \psi^{(2)} \right] dV = 0 \tag{4.35}$$

where t_i' is used to denote modified surface tractions due to the inclusion of a portion of the stress tensor within f_i', as indicated in (4.14). Note that in equation (4.35), once again, the * indicates a Riemann convolution integral in time.

4.3.4 Boundary Integral Equation

By introducing the $^{(1)}$ states corresponding to that given by fundamental solution (unit body force and unit heat source) in the above equation, one obtains the following integral representation for the surface velocity:

$$c_{\beta\alpha}(\xi) v_\beta(\xi,\tau) = \int_s \left[\dot{G}_{\beta\alpha} * t_\beta'(X,t) - \dot{F}_{\beta\alpha} * v_\beta(X,t) \right] dS(X)$$

$$+ \int_v \left[\dot{G}_{\beta\alpha} * f_\beta'(Z,t) \right] dV(Z) \tag{4.36}$$

where in two-dimensions

$$v_\beta = [v_1 \; v_2 \; \theta]^T$$

$$t_\beta' = [t_1' \; t_2' \; q]^T$$

$$f_\beta' = [f_1' \; f_2' \; \;]^T .$$

As in thermoelasticity, the Greek subscripts range from one to d+1, where d is the dimensionality of the problem. Next, perform integration by parts

on the third term in f_i' to rewrite the boundary integral in terms of total tractions t_i. The result can be written as

$$c_{\beta\alpha}(\xi)v_\beta(\xi,\tau) = \int_S \left[\dot{G}_{\beta\alpha} * t_\beta(X,t) - \dot{F}_{\beta\alpha} * v_\beta(X,t) \right] dS(X)$$

$$+ \int_V \left[\frac{\partial \dot{G}_{ij}}{\partial x_i} \delta_{j\alpha} * p_v(Z,t) + \dot{G}_{\beta\alpha} * f_\beta(Z,t) \right] dV(Z) \qquad (4.37)$$

where

$$t_\beta = [t_1 \; t_2 \; q]^T$$

$$f_\beta = [f_1 \; f_2 \; \;]^T$$

$$p_v = \rho_v R\Theta$$

$$f_i = \rho \frac{\partial v_i}{\partial t} + \rho v_j \frac{\partial v_i}{\partial x_j} .$$

$$\delta_{j\alpha} = \begin{cases} 1 & \text{for } j = \alpha \\ 0 & \text{for } j \neq \alpha \end{cases}$$

The volume integral in (4.37) can be condensed further and expressed as:

$$c_{\beta\alpha}(\xi)v_\beta(\xi,\tau) = \int_S \left[\dot{G}_{\beta\alpha} * t_\beta(X,t) - \dot{F}_{\beta\alpha} * v_\beta(X,t) \right] dS(X)$$

$$+ \int_V \left[\dot{Q}_\alpha * p_v(Z,t) + \dot{G}_{\beta\alpha} * f_\beta(Z,t) \right] dV(Z) \; . \qquad (4.38)$$

For interior quantities, velocities can be computed from (4.38) with $c_{\beta\alpha} = \delta_{\beta\alpha}$, and additionally,

$$\frac{\partial v_\alpha}{\partial x_i}(\xi,\tau) = \int_S \left[\dot{E}_{\beta\alpha i} * t_\beta(X,t) - \dot{D}_{\beta\alpha i} * v_\beta(X,t) \right] dS(X)$$

$$+ \int_V \left[\dot{P}_{\alpha i} * p_v(Z,t) + \dot{E}_{\beta\alpha i} * f_\beta(Z,t) \right] dV(Z) + J_{\alpha i} p_v(\xi,\tau)$$

where $J_{\alpha i}$ is a discontinuity term arising out of the treatment of the improper volume integral involving $P_{\alpha i}$. Meanwhile, the interior velocity

and temperature rates can be computed from:

$$\frac{\partial v_\alpha}{\partial t}(\xi,\tau) = \int_S \left[\dot{\dot{G}}_{\beta\alpha} * t_\beta(X,t) - \dot{\dot{F}}_{\beta\alpha} * v_\beta(X,t) \right] dS(X) + \int_V \left[\dot{\dot{G}}_{\beta\alpha} * f_\beta(Z,t) \right] dV(Z) .$$

4.4 Numerical Implementation

4.4.1 Surface and Volume Integrations

The numerical treatment of the equations in fluid dynamics coupled with heat transfer follows very closely that described in Section 3 for transient thermal stress analysis. Interestingly, all of the singularities of the functions G and F on the boundaries, as well as, in the interior are identical. However, now the volume must be subdivided into cells. The geometry of each cell is again defined by nodal points and quadratic shape functions. In two-dimensions, six and eight-noded cells are available. The quadratic geometric variation permits representation of intricate shapes with a minimal number of cells. Meanwhile, either a linear or quadratic variation can be employed for the functional representation. Formally, then, for any cell,

$$Z(\zeta) = z_i(\zeta) = M_w(\zeta) z_{iw}$$

$$f_\alpha(\zeta) = M_\omega(\zeta) f^n_{\alpha\omega}$$

where

ζ intrinsic coordinates

M_w, M_ω shape functions

z_{iw} nodal coordinates of cell

$f^n_{\alpha\omega}$ nodal value of body force .

In the above, the index w varies from one to the number of geometric nodes, while ω ranges from one to the number of functional nodes in the cell under consideration. With this spatial discretization in mind, the integral equations can now be rewritten. For the generalized velocity this becomes

$$c_{\beta\alpha}(\xi)v^N_\beta(\xi) = \sum_{n=1}^{N}\{\sum_{m=1}^{M}[\, t^n_{\beta\omega}\int_{S_m} G^{N+1-n}_{\beta\alpha}(X(\zeta)-\xi)N_\omega(\zeta)dS(\zeta))$$

$$- v^n_{\beta\omega}\int_{S_m} F^{N+1-n}_{\beta\alpha}(X(\zeta)-\xi)N_\omega(\zeta)dS(X(\zeta))\,]$$

$$+\sum_{m=1}^{L}[\, f^n_{\beta\omega}\int_{V_m} G^{N+1-n}_{\beta\alpha}(Z(\zeta)-\xi)M_\omega(\zeta)dV(Z(\zeta))\,]\,\}$$

where

$$V = \sum_{m=1}^{L} V_m$$

and L is the number of volume cells. A similar expression results for the strain rates. The integration techniques required for the evaluation of the surface integrals have been discussed in Section 3.4.4. For volume integration, as in the surface integration techniques, subsegmentation and variable quadrature order are used to control error with separate schemes employed for singular and non-singular cases. Specific details on this volume integration algorithm can be found in Mustoe (1984), Raveendra (1984), and Banerjee and Raveendra (1986).

The explicit form of the kernel functions $G_{\beta\alpha}$, $F_{\beta\alpha}$, $E_{\beta\alpha i}$ and $D_{\beta\alpha i}$ have been developed for the two-dimensional case and are presented in Appendix C. As would be expected, these functions reduce to within a spatially independent constant of their steady-state counterparts when $t \rightarrow \infty$. Furthermore, in a manner identical to that described for the thermoelastic solid, these kernels decompose into a singular steady-state portion plus a

non-singular transient component.

4.4.2 The Treatment of Continuity Equation

The continuity equation for a compressible flow takes the role of the elastoplastic constitutive equation in solid mechanics. Recalling the continuity equations

$$\rho = \rho_r + \rho_v \tag{4.39a}$$

$$\frac{\partial \rho}{\partial t} + v_j \frac{\partial \rho}{\partial x_j} + \rho \frac{\partial v_j}{\partial x_j} = 0 \tag{4.39b}$$

where ρ is the density.

It is necessary to satisfy these equations at discrete nodal points. By defining a global shape function, the density variation can be interpolated as

$$\rho(x^l) = \sum_{m=1}^{M} C(x^l, \xi^m)\emptyset(\xi^m) \qquad \text{for } l = 1,2,\ldots,M \tag{4.40}$$

where $C(x^l, \xi^m) = 1 - \frac{r}{r_{max}}$ where $r = (y_i y_i)^{1/2}$ and $y_i = x_i^l - \xi_i^m$

r_{max} = the maximum distance between any two points of the region.

In order to satisfy (4.39), the values of ρ (or ρ_v), $\partial\rho/\partial x_j$, v_j and $\partial v_j/\partial x_j$ must be calculated. Of these, v_j and $\partial v_j/\partial x_j$ are obtained directly from the boundary or interior integral representations. The value of ρ or ρ_v is obtained from (4.40) and its gradient is calculated via

$$\frac{\partial \rho}{\partial x_j}(x^l) = \sum_{m=1}^{M} D_j(x^l, \xi^m)\emptyset(\xi^m) \tag{4.41}$$

where

$$D_j(x^l,\xi^m) = \frac{\partial C(x^l,\xi^m)}{\partial x_j} = -\frac{1}{r_{max}}\left(\frac{y_j}{r}\right)$$

By utilizing the known values at time t in the continuity equation, the unknown density at t+Δt can be obtained assuming a Crank-Nicolson type γ-algorithm. Thus:

$$[L_{lm}]\{\phi_m\} = \{R_l\} \tag{4.42}$$

where

$$L_{lm} = \left[\frac{1}{\Delta t} + \gamma^{t+\Delta t}\frac{\partial v_j}{\partial x_j}(x^l)\right]C^{lm} + \left[\gamma^{t+\Delta t}v_j(x^l)\right]D_j^{lm}$$

$$R_l = \left[\frac{1}{\Delta t} + (\gamma-1)^t\frac{\partial v_j}{\partial x_j}(x^l)\right]^t\rho + \left[(\gamma-1)^t v_j(x^l)\right]^t\frac{\partial \rho}{\partial x_j}$$

Once $\{\phi_m\}$ is determined, the required quantities ${}^{t+\Delta t}\rho(x^l)$ and ${}^{t+\Delta t}\frac{\partial \rho}{\partial x_j}(x^l)$ can be computed from (4.40) and (4.41).

4.4.3 Algorithm for Incremental Iterative Solution

The final system of algebraic equations resulting from the previous integral representations can be expressed as

$$A^b x - G^b f = B^b y \tag{4.43a}$$

$$v = A^v x + B^v y + G^v f \tag{4.43b}$$

$$\dot{v} = \dot{A}^v x + \dot{B}^v y + \dot{G}^v f \tag{4.43c}$$

$$\varepsilon = A^\varepsilon x + B^\varepsilon y + G^\varepsilon f \tag{4.43d}$$

where

x,y are the known and unknown boundary quantities

$\dot{v}$,v are the velocity and acceleration vectors

ε are velocity gradients

An iterative algorithm similar to the initial stress method (Banerjee and Butterfield, 1981) can then be developed as follows:

1. Increment boundary conditions
2. Assume f = 0
3. Calculate the boundary and interior solutions x,v,$\dot{v}$ and ε
4. Determine f, ψ, and ρ_v at this time increment
5. Calculate the boundary and interior solutions again
6. If the solution is not significantly different from (3), go to (1); if the solution is different, then go to (4).

4.4.4 Algorithm for Direct Solution

Just as the finite element method can be used to obtain the solution of a nonlinear system either iteratively or directly using incrementally updated system equations, analogous techniques can be developed for the boundary element method. The direct BEM algorithm was developed recently for elastoplasticity by Banerjee and Raveendra (1987) and Henry and Banerjee (1988). For the computational fluid dynamics problem the same underlying principle can also be used to develop a direct algorithm. Equations (4.43) can be rewritten for this purpose as:

$$A^b x + B^b y + G^b f = 0 \tag{4.44a}$$

$$\varepsilon - A^\varepsilon x - B^\varepsilon y + G^\varepsilon f = 0 \tag{4.44b}$$

By pre multiplying (4.44b) by v^T one obtains

$$v^T\varepsilon - v^T A^\varepsilon x - v^T B^\varepsilon y + v^T G^\varepsilon f = 0 \ . \tag{4.45}$$

Noting that $v^T\varepsilon = f$, (4.45) and (4.44a) combine to produce

$$\begin{bmatrix} A^b & G^b \\ v^T A^\varepsilon & I - v^T G^\varepsilon \end{bmatrix} \begin{Bmatrix} X \\ f \end{Bmatrix} = \begin{Bmatrix} B^b y \\ v^T B^\varepsilon y \end{Bmatrix} \tag{4.46}$$

Equation (4.46) can be solved directly if v, ρ_v or ρ can be estimated for the next increment. This does, of course require at least one iteration.

If substructuring is necessary, the above equation can be expressed for a problem involving n subregions as:

$$\begin{bmatrix} A_{11} & -G_1^f & A_{12} & 0 & \cdots & A_{1n} & 0 \\ v^T A_1 & (I - v^T G_1^f & 0 & 0 & \cdots & 0 & 0 \\ A_{21} & 0 & A_{22} & -G_2^f & \cdots & A_{2n} & 0 \\ 0 & 0 & v^T A_2 & (I - v^T G_2^f) & \cdots & 0 & 0 \\ \vdots & \vdots & \vdots & \vdots & \vdots & \vdots & \vdots \\ A_{n1} & 0 & A_{n2} & 0 & \cdots & A_{nn} & -G_n^f \\ 0 & 0 & 0 & 0 & \cdots & v^T A_n & (I - v^T G_n^f) \end{bmatrix} \begin{Bmatrix} x_1 \\ f_1 \\ x_2 \\ f_2 \\ \vdots \\ x_n \\ f_n \end{Bmatrix} = \begin{Bmatrix} b_{1x} \\ b_{1f} \\ b_{2x} \\ b_{2f} \\ \vdots \\ b_{nx} \\ b_{nf} \end{Bmatrix}$$

This block banded set of equations must be formulated and decomposed on each iteration.

4.5 Examples of Viscous Flow Analysis

4.5.1 Introduction

The various fluid formulations, described in the foregoing, are in various stages of development. For incompressible flow, both iterative and direct algorithms have been implemented, although validation has been completed only under steady-state conditions. On the other hand, the compressible flow formulation has again been implemented, but serious testing of the algorithm awaits completion of the new time-dependent

compressible kernels mentioned in Section 4.3.2.

In the following subsections, several examples are presented to demonstrate the validity of the present boundary element formulations.

4.5.2 Driven Cavity

The two-dimensional driven cavity has become the standard test problem for incompressible computational fluid dynamics codes. In a way, this is unfortunate because of the ambiguities in the specification of the boundary conditions. However, numerous results are available for comparison purposes.

The incompressible fluid of uniform viscosity is confined within a unit square region. The fluid velocities on the left, right and bottom sides are fixed at zero, while a uniform non-zero velocity is specified in the x-direction along the top edge. Normal (y-direction) velocity is also zero on the top surface. Thus, in the top corners, the x-velocity is not clearly defined. To alleviate this difficulty in the present analysis, this velocity component is smoothed out as indicated in Figure 4.2. Additionally, steady-state conditions have been assumed and the forcing velocity is slowly incremented to achieve the desired Reynolds number.

Several levels of mesh refinement, as shown in Figure 4.3, were examined to determine the effect on accuracy and convergence. Spatial plots of the resulting velocity vectors for the twenty-four cell model are presented in Figure 4.4 for Reynolds numbers (Re) of 0, 100 and 250. Meanwhile, Figure 4.5 contains the velocity distribution along the vertical cavity centerline. All of these results correlate closely with those obtained by Burggraf (1966) in his classic paper on steady separated flows. However, as Re increases, the convective terms begin to dominate the viscous ones, and then problems with numerical instability arise. In the

current boundary element analysis, results diverge as Re reaches a certain value dependent, initially, upon mesh refinement. Beyond a certain level of mesh refinement, though, no improvement was found. Table 4.1 contains the approximate Reynolds number at divergence for the various cell patterns displayed in Figure 4.3. Additionally, decreased increment size and/or increased number of iterations had little effect on the divergent character of this problem.

The thirty-six cell model was also run as a three region problem as defined in Figure 4.6. This dramatically reduced computing time, since now integration is limited to within each individual region. At low Re, results were quite good, thus verifying the multi-GMR approach. Convergence was enhanced to the extent that solutions could be attained up to Re = 300. Figure 4.7 contains velocity vector plots at Re = 250, 300, and 325. The latter is an unconverged result. Notice the disturbances entering the solution near the center of the cavity.

Next, the direct algorithm described in Section 4.4.4 was utilized for the same problem. In this case, computational effort increased dramatically, since interior forces are added to the list of primary unknowns. While convergence was generally achieved with only a few iterations in the lower Reynolds number range, the divergent character of the solution process remained unaltered. That is, even with a fine mesh, divergence occurred at approximately Re = 300.

Interestingly, the same phenomenon occurs in both finite difference and finite element approaches in approximately the same Reynolds number range. In these methods, upwinding schemes (Allen and Southwell, 1955; Henrich and Zienkiewicz, 1979) and artificial dissipation (Hughes et al, 1979) have been devised to enhance convergence. This would occur almost automatically in a transient boundary element formulation because these

upwinding schemes and dissipations are part of the transient solutions. As an initial test of the transient formulation, the cavity was examined with an abrupt jump in velocity along the upper edge at time zero. Results at four different time steps, for $R_e = 100$, are shown on Figure 4.8. Notice that eventually the steady-state solution is achieved.

4.5.3 Buoyancy Driven Flow

The domain is again the unit square cavity. Velocity is zero on all boundaries, while the top and bottom edges are insulated. The temperature of the right edge is maintained at zero, but the left face temperature is slowly elevated under steady-state conditions. By including the body forces due to buoyancy, the existing temperature gradients produce free convection within the cavity. The resulting steady-state velocity vector distribution for a Grashof number of 100 is presented in Figure 4.9, while the corresponding temperature variation along three vertical planes is plotted in Figure 4.10. Again, in a manner similar to that encountered in the previous example, convergence difficulties arise in the steady state case as the temperature gradients (i.e., the Grashof number) are elevated beyond a critical value. A transient solution would probably not have the same difficulty.

4.5.4 Unconfined Flow Around Obstacles

Boundary element models have been constructed for flow around a simplified blade as shown in Figure 4.11. Preliminary results have been obtained. This problem will be investigated more thoroughly in the next few months.

4.6 Discussion

Obviously, based upon the results of the numerical studies presented in the previous subsection, significant improvements in the current

boundary element implementation for the fluid are still needed. First of all, the recent introduction of the time-dependent kernel functions described in Section 4.3 should help considerably. With time dependence, as Reynolds number increases the transition is from parabolic to hyperbolic behavior, rather than from elliptic to hyperbolic. From a numerical standpoint, this is much more forgiving. In fact, it is not surprising that most finite difference and finite element approaches to steady-state flows utilize either a real or psuedo time stepping approach.

Secondly, the introduction of compressibility into the system should have a positive effect. Experience in plasticity, for example, has indicated that more accurate solutions are attainable for compressible materials. In addition, there is considerable room for improvement in the non-linear solution algorithms. Presently, only simple iteration has been investigated, however, implicit schemes, Newton-Raphson methods, and optimization techniques may prove beneficial.

FIGURE 4.1

FUNDAMENTAL SOLUTION

Spherical Coordinate System

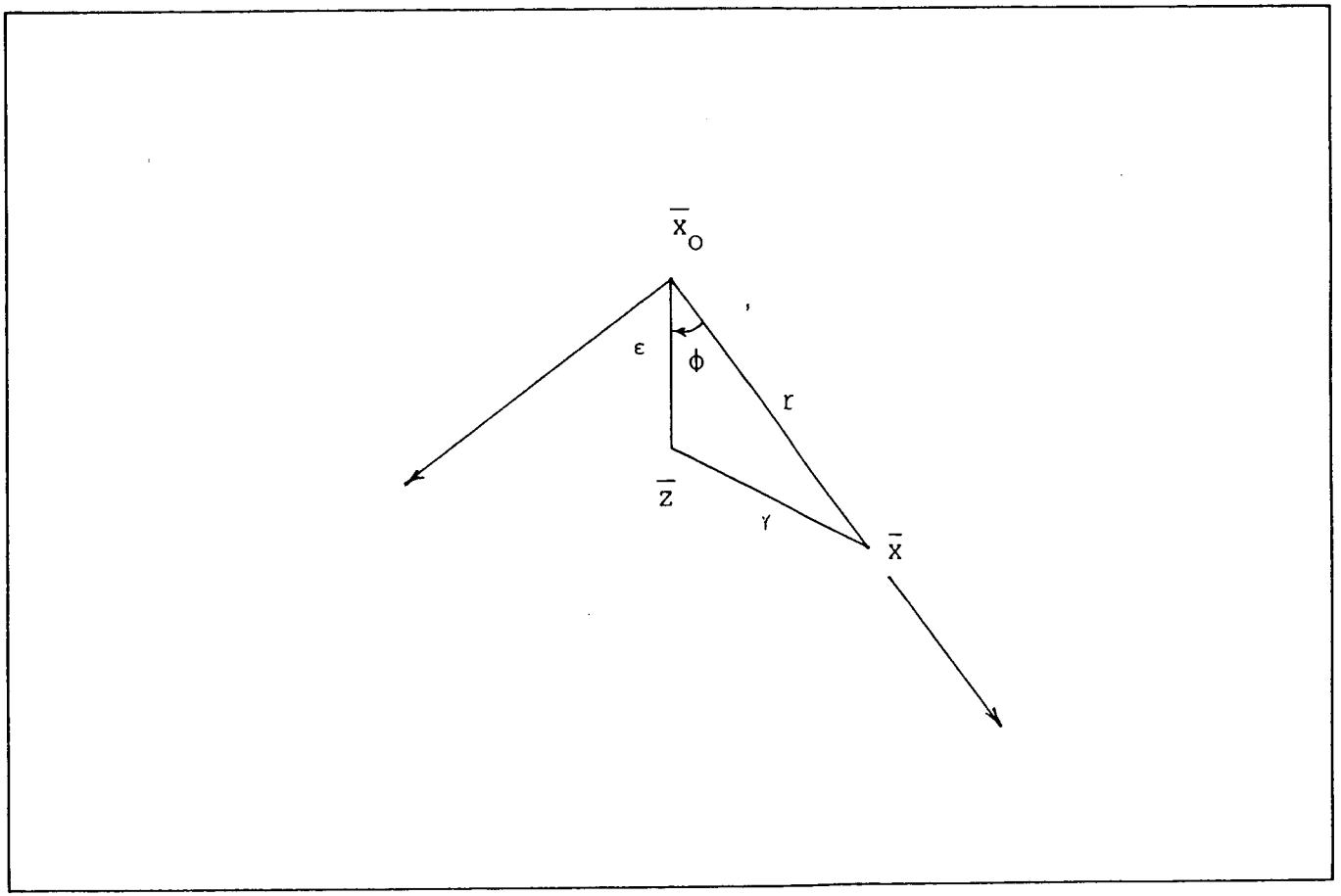

FIGURE 4.2 - DRIVEN CAVITY PROBLEM DEFINITION

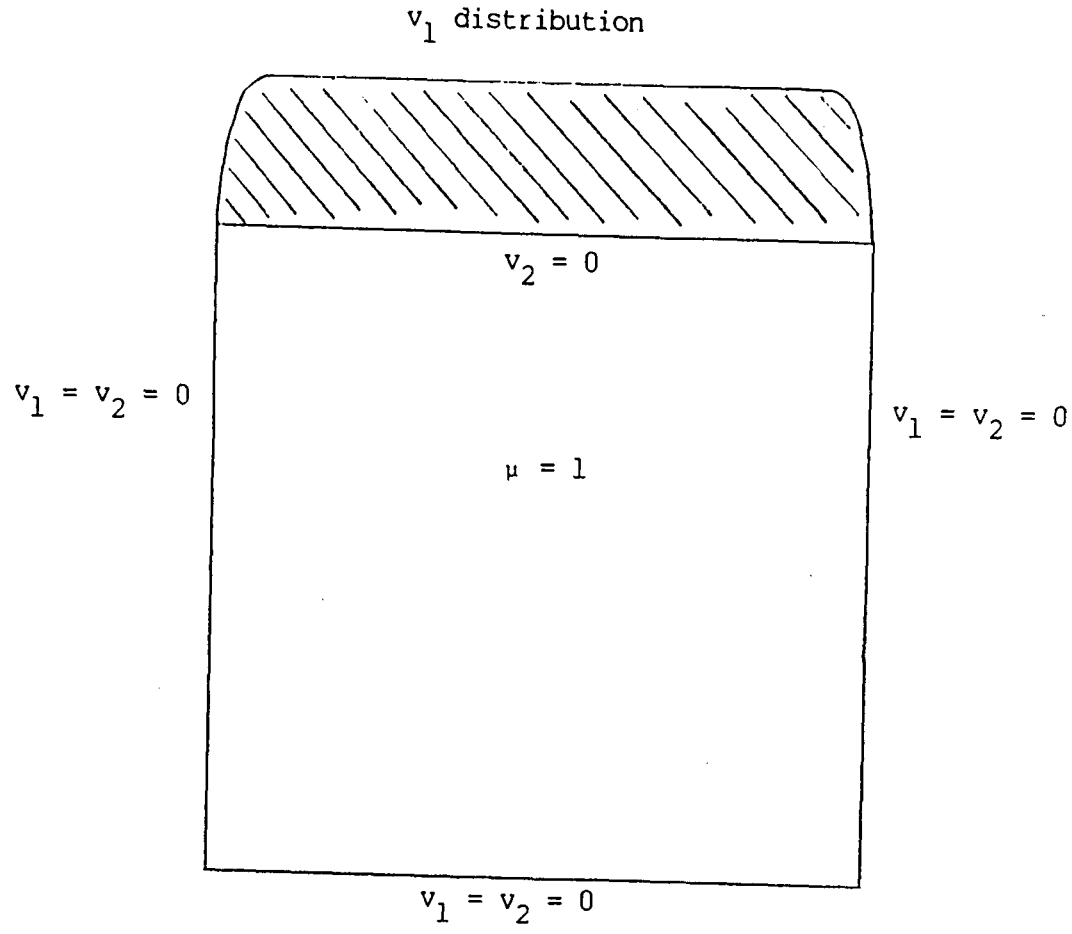

FIGURE 4.3 - DRIVEN CAVITY BOUNDARY ELEMENT MODELS

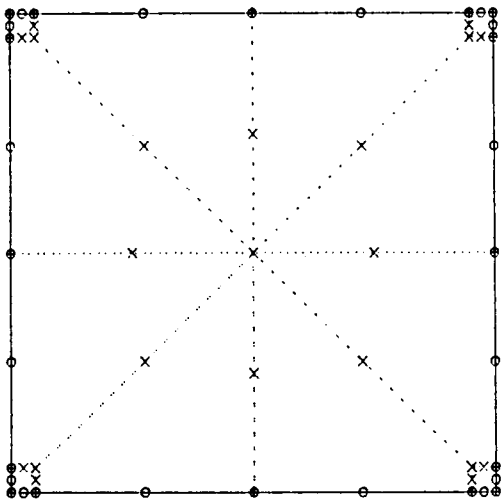

a) Twelve Cell Model

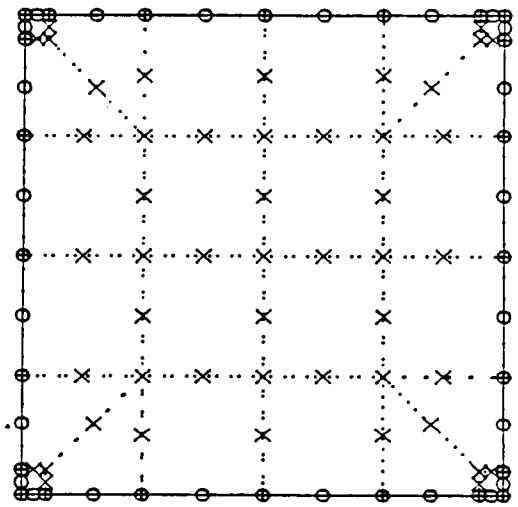

b) Twenty-four Cell Model

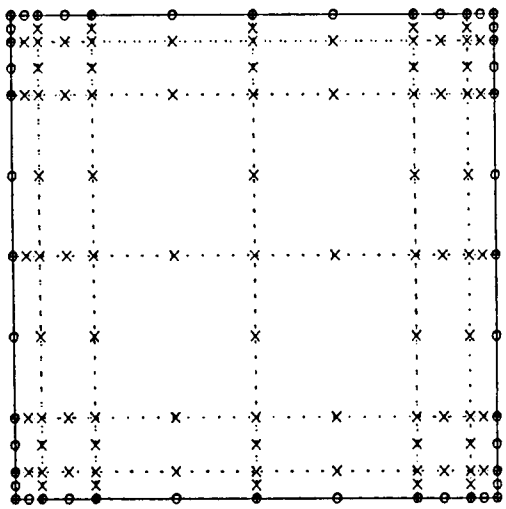

c) Thirty-six Cell Model

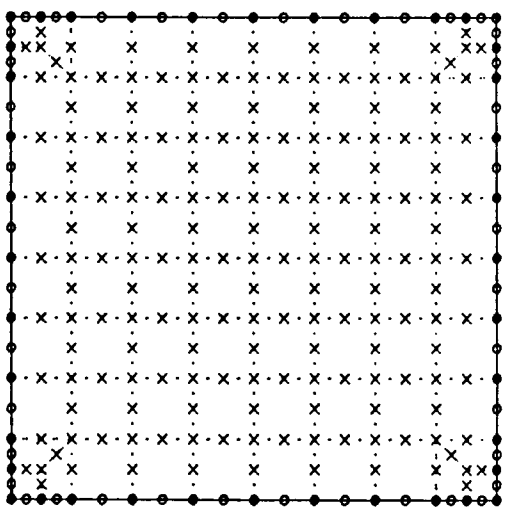

d) Seventy-two Cell Model

FIGURE 4.4 - DRIVEN CAVITY VELOCITY DISTRIBUTION

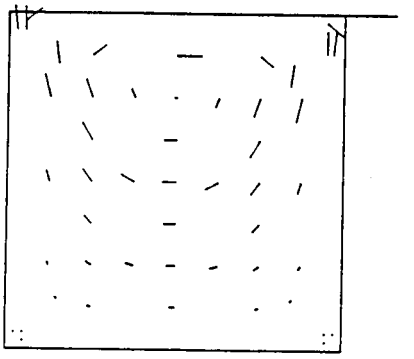

a) Re = 0

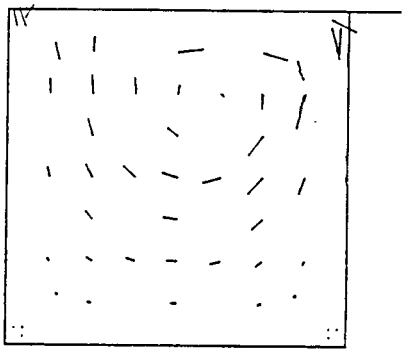

b) Re = 100

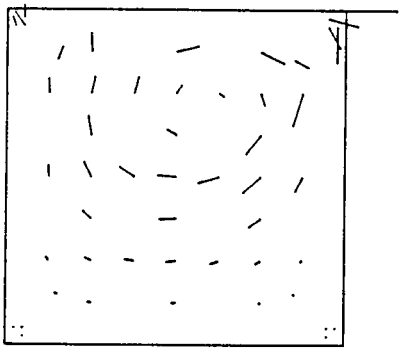

c) Re = 250

FIGURE 4.5

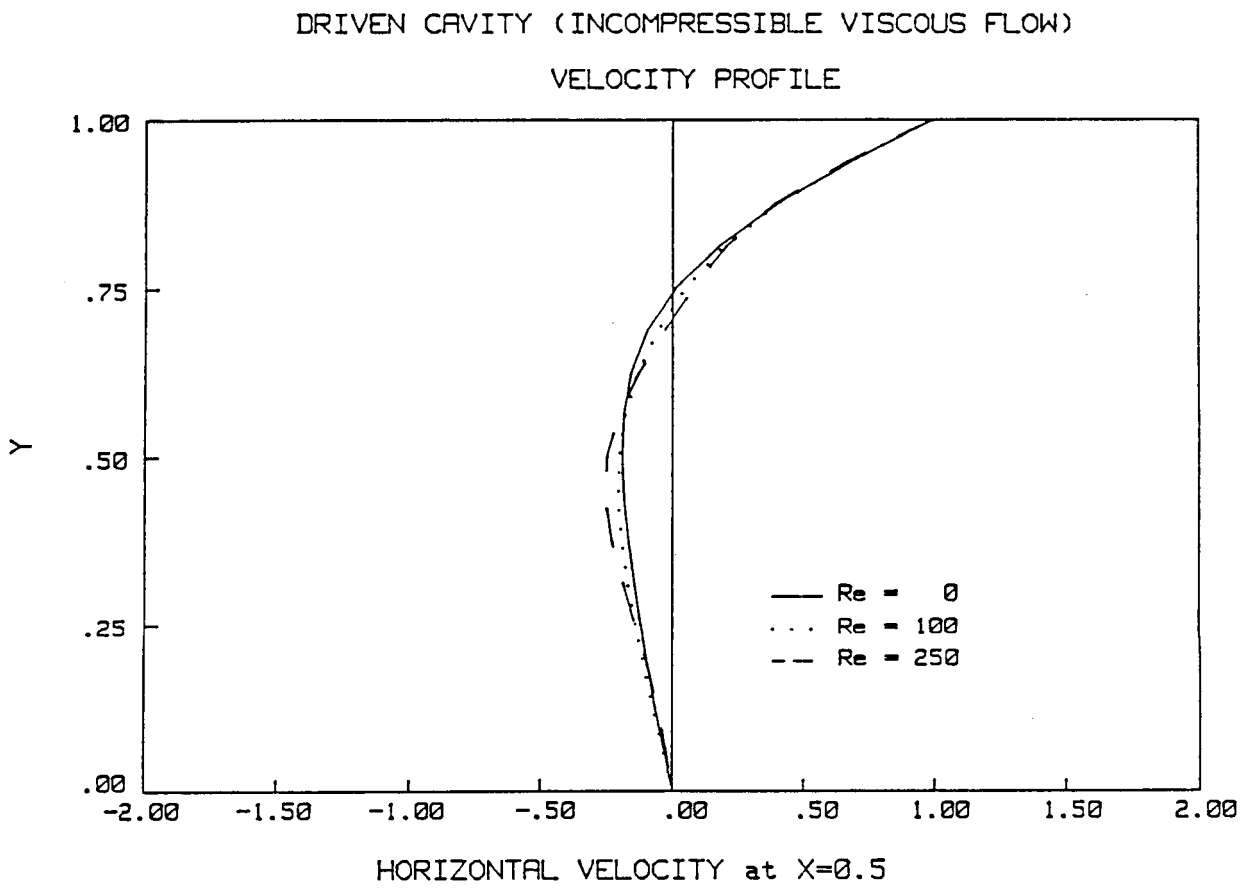

TABLE 4.1 - DRIVEN CAVITY DIVERGENCE CHARACTERISTICS

Mesh Refinement (Number of Cells)	Approximate Re at Divergence
8	30
12	65
24	260
36	260
72	250

FIGURE 4.6 - DRIVEN CAVITY (THREE REGION, THIRTY-SIX CELL MODEL)

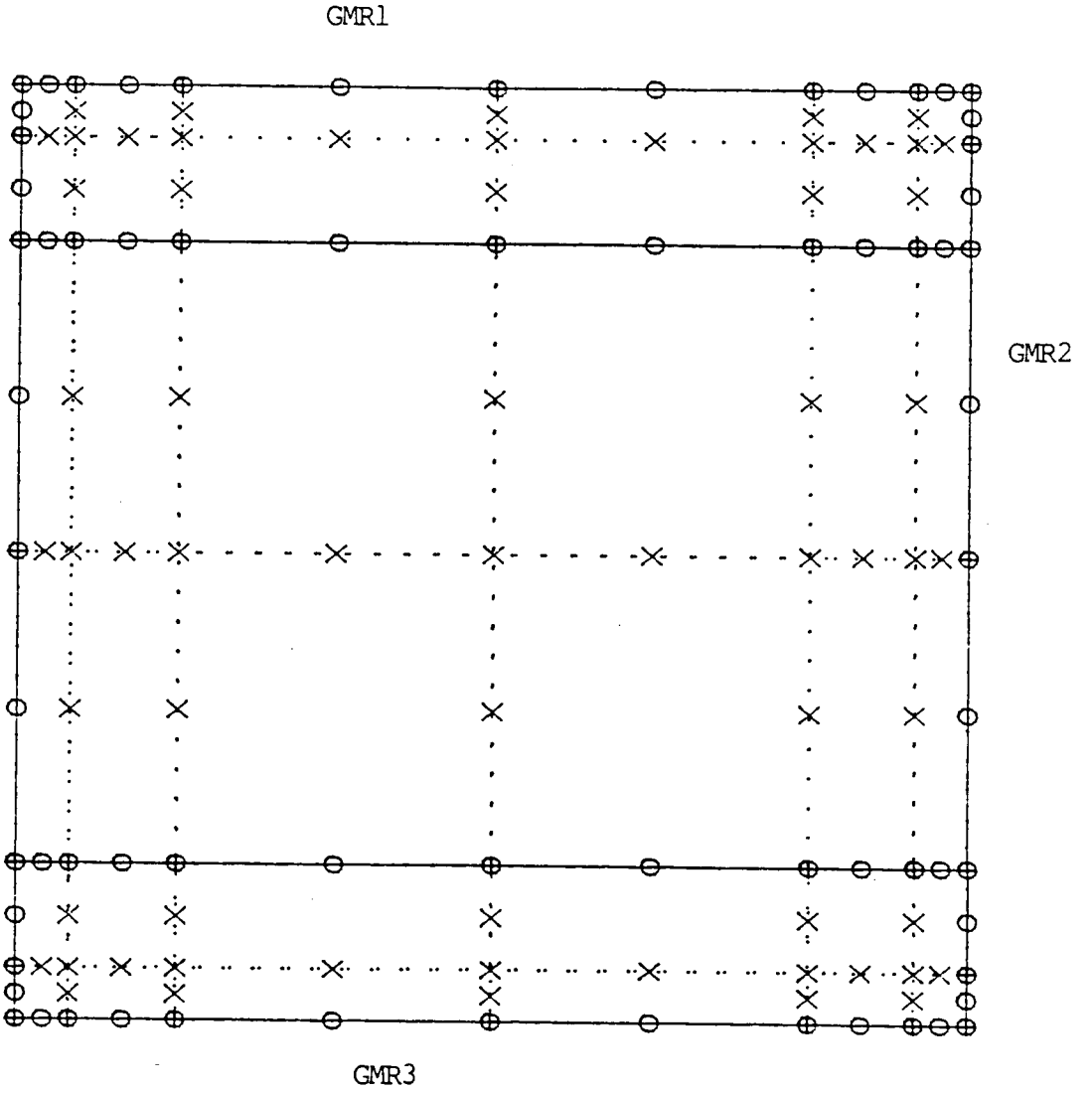

FIGURE 4.7 - DRIVEN CAVITY VELOCITY DISTRIBUTION (THREE REGION MODEL)

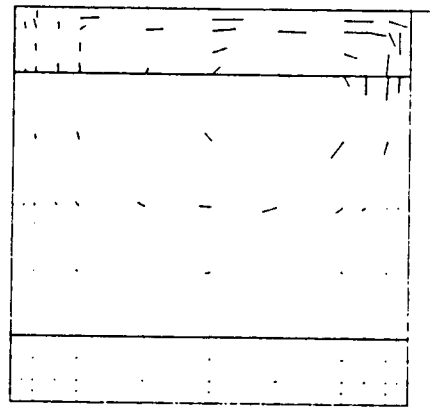

a) Re = 250

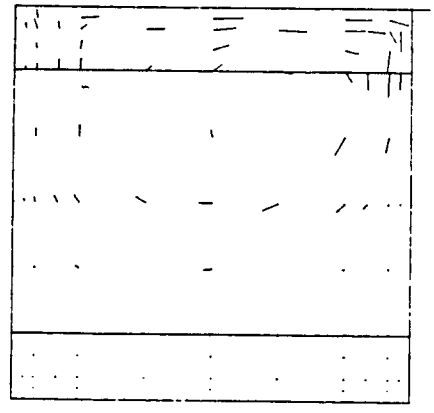

b) Re = 300

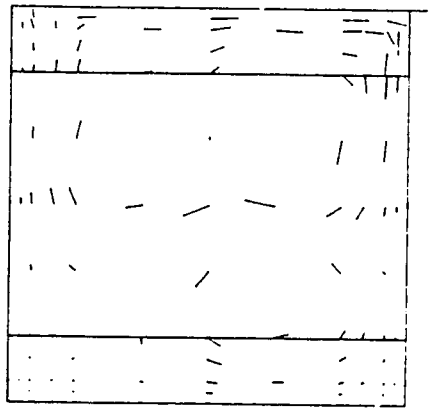

c) Re = 325 (unconverged)

FIGURE 4.8 - DRIVEN CAVITY - TRANSIENT RESPONSE

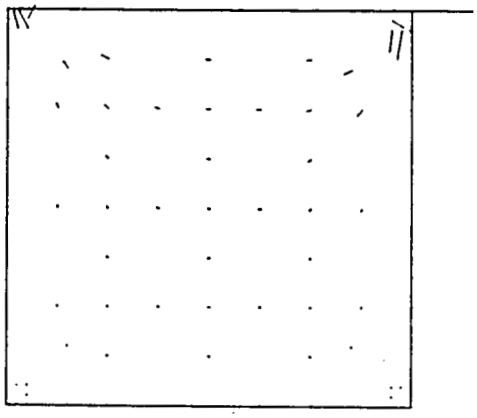

t = 0.001

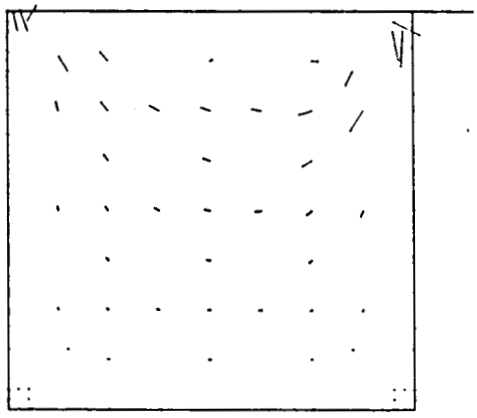

t = 0.005

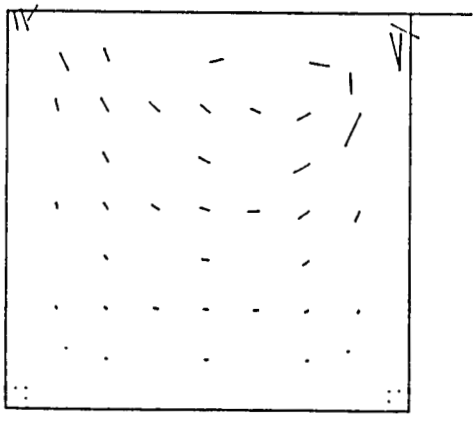

t = 0.020

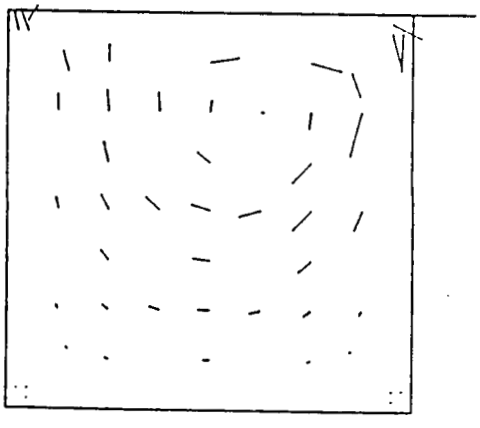

t = 0.050

FIGURE 4.9

BUOYANCY DRIVEN CAVITY

VELOCITY DISTRIBUTION

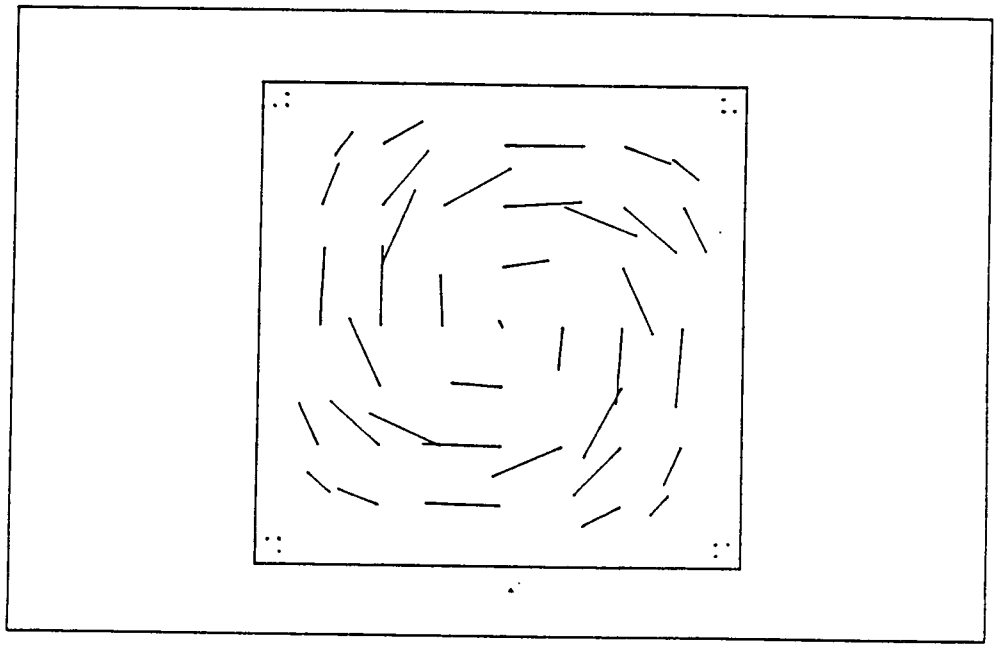

FIGURE 4.10

BUOYANCY DRIVEN CAVITY

TEMPERATURE PROFILE

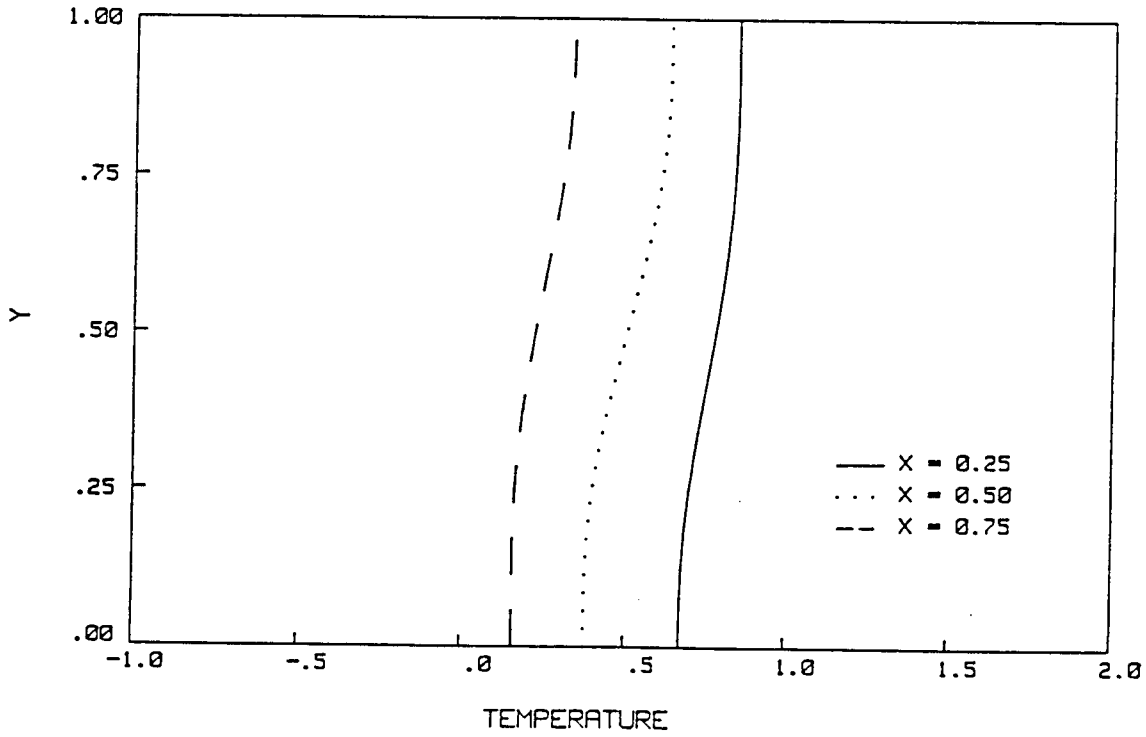

FIGURE 4.11 - FLOW AROUND A SIMPLIFIED BLADE

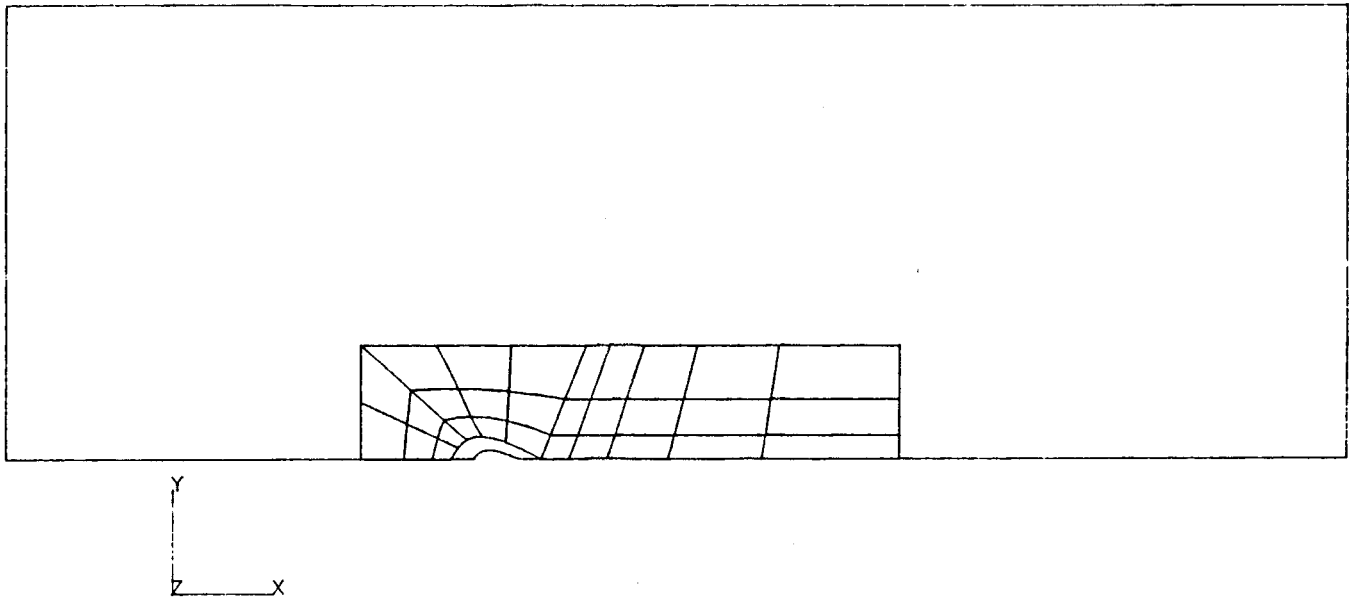

5. SUMMARY OF PROGRESS

As is evident from the previous two sections, significant progress has been made toward the goal of developing a general purpose boundary element method for hot fluid-structure interaction. For the solid phase, a boundary-only formulation was developed and implemented for uncoupled transient thermoelasticity in two dimensions. The elimination of volume discretization not only drastically reduces required modeling effort, but also permits unconstrained variation of the through-the-thickness temperature distribution. Consequently, it is expected that this formulation can provide an attractive alternative to finite element methods for transient thermal stress analysis, particularly when accurate stresses are required. It should be noted that the BEM detailed in Section 3 is the first boundary-only implementation for this class of problems.

Meanwhile, for the fluid, significant strides have also been made. Fundamental solutions have been derived for transient incompressible and compressible flow in the absence of the convective terms. Boundary element formulations have been developed as well and were described in Section 4. For the incompressible case, the necessary kernel functions, under transient and steady-state conditions, have been derived and fully implemented into a general purpose, multi-region boundary element code. Several examples have been examined in detail to study the suitability and convergence characteristics of the various algorithms.

While considerable effort is still needed to produce a useful analytical tool for high Reynolds number hot gas flow, the development to date does represent a substantial advancement in the state-of-the-art. Table 5.1 is provided in order to highlight the status of the major components of the overall hot fluid-structure interaction program.

TABLE 5.1 Program Status

Category	Integral Formulation	Kernel Development	General Purpose Implementation	Validation
SOLID				
Thermoelastic (Uncoupled, Quasistatic)	Completed	Completed	Completed	Completed
FLUID (non-isothermal)				
Steady, Incompressible	Completed	Completed	Completed	Completed
Time-dependent, Incompressible	Completed	Completed	Completed	In-progress
Time-dependent, Compressible	Completed	In-Progress	In-Progress	Future

6. WORKPLAN FOR THE NEXT YEAR

The following tasks are planned, in approximate chronological order, for the period November 1987 - March 1989:

1. Complete the time-dependent compressible flow kernel development and general-purpose implementation.
2. Begin validation of the time-dependent formulations. After the initial debugging phase, download the code to the NASA Cray for this task.
3. Investigate enhanced non-linear solution algorithms for Navier-Stokes flow.
4. Develop and implement a thermally-sensitive inviscid, compressible flow formulation.
5. Implement interface coding for fluid-solid interaction.
6. Assess suitability for large scale development of boundary element methods for hot fluid-structure interaction.

APPENDICES

APPENDIX A - REFERENCES

Ahmad, S., (1986), Linear and Nonlinear Dynamic Analysis by BEM, Ph.D. Dissertation, State University of New York at Buffalo.

Allen, D. and Southwell, R.V. (1955), 'Relaxation Methods Applied to Determine the Motion, in Two Dimensions, of a Viscous Fluid Past a Fixed Cylinder,' Q.J. Mech. Appl. Math., V8, pp. 129-145,

Banerjee, P.K. and Butterfield, R. (1981), 'Boundary Element Methods in Engineering Science,' McGraw-Hill, London.

Banerjee, P.K. and Butterfield, R. (1979), 'Developments in Boundary Element Methods-1,' Elsevier Applied Science Publishers, London.

Banerjee, P.K. and Mukherjee, S. (1984), 'Developments in Boundary Element Methods-3,' Elsevier Applied Science Publishers, London.

Banerjee, P.K. and Raveendra, S.T. (1986) 'Advanced Boundary Element of Two- and Three-dimensional Problems of Elasto-plasticity,' Int. J. Num. Meth. Engrg., V23, pp. 985-1002.

Banerjee, P.K. and Raveendra, S. (1987), 'A New BEM Formulation for 2D Elastoplastic Analysis,' Journal of Engineering Mechanics.

Banerjee, P.K. and Shaw, R.P. (1982), 'Developments in Boundary Element Methods-2,' Elsevier Applied Science Publishers, London.

Banerjee, P.K. and Watson, J.O. (1986), 'Developments in Boundary Element Methods-4,' Elsevier Applied Science Publishers, London.

Banerjee, P.K., Wilson, R.B. and Miller, N. (1985), 'Development of a Large BEM System for Three-dimensional Inelastic Analysis,' in Advanced Topics in Boundary Element Analysis, ed. T.A. Cruse, A.B. Pifko and H. Armen, AMD-V72, ASME, New York.

Boley, B.A. and Weiner, J.H. (1960), 'Theory of Thermal Stresses,' John Wiley and Sons, New York.

Burggraf, O.R. (1966), 'Analytical and Numerical Studies of the Structure of Steady Separated Flows,' J. Fluid Mech., V24, Part 1, pp. 113-151.

Bush, M.B., Milthorpe, J.F. and Tanner, R.I. (1984), 'Finite Element and Boundary Element Methods for Extrusion Computations,' J. Non-Newtonian Fluid Mech., Vol. 16, 37-51.

Bush, M.B. and Tanner, R.I. (1983), 'Numerical Solution of Viscous Flow Using Integral Equation Methods,' Int. J. Num. Meth. Fluids, Vol. 3, 71-92.

Choquin, J.P. and Huberson, S. (1986), 'Numerical Simulation of Viscous Flows Using Particle Methods,' pp. 297-302 in R.P. Shaw et.al., Eds., Proc. 4th Intl. Symp. Innov. Num. Methods Engrg., Springer, Berlin.

Chung, T.J. (1978), 'Finite Element Analysis in Fluid Dynamics,' McGraw Hill, New York.

Coleman, C.J. (1984), 'On the Use of Boundary Integral Methods in the Analysis on Non-Newtonian Fluid Flow,' J. Non-Newtonian Fluid Mech., Vol. 16, 347-355.

Coulmy, G. (1976), 'An Extension of the Discrete Singularities Distribution Method for the Computation of Velocity Fields with Nonzero Divergence or Curl,' in Proc. Euromech. Colloquium 75, Braunschweig, Germany.

Cruse, T.A. (1974), 'An Improved Boundary Integral Equation Method for Three-Dimensional Elastic Stress Analysis,' Comp. and Struct., V4, pp. 741-754.

Dargush, G.F. (1987), BEM for the Analogous Problems of Thermoelasticity and Soil Consolidation, Ph.D. Dissertation, State University of New York at Buffalo.

Dongarra, J.J. et al (1979), Linpak User's Guide, SIAM, Philadelphia.

El Refaee, M.M., Wu, J.C., and Lekoudis, S.G. (1981), 'Solution of Compressible Navier-Stokes Equations Using the Integral Method,' AIAA Journal, Vol. 20, 356-362.

Gunn, M.J. and Britto, A.M. (1984), CRISP User's and Programmer's Guide, Engineering Department, Cambridge University.

Heinrich, J. and Zienkiewicz, O.C. (1979), 'The Finite Element Method and 'Upwinding' Techniques in the Numerical Solution of Convection Dominated Flow Problems,' pp. 105-136 in T.J.R. Hughes, Editor, Finite Element Methods for Convection Dominated Flows, ASME, AMD-Vol. 34, New York.

Henry, D.P. and Banerjee, P,K. (1988) 'A Variable Stiffness Type BEM Formulation for Axisymmetric Elastoplasticity,' to appear in Int. Jour. Num. Methods in Engrg.

Hughes, T.J.R., Liu, W.K., and Brooks, A. (1979), 'Finite Element Analysis of Incompressible Viscous Flows by the Penalty Function Formulation,' J. Comp. Physics, V30, pp. 1-60.

Latchat, J.C. and Watson, J.O. (1976), 'Effective Numerical Treatment of Boundary Integral Equations: A Formulation for Three-dimensional Elastostatics,' Int. J. Num. Meth. Engrg., V10, pp. 991-1005.

Morino, L. and Piva, R. (1987) 'Boundary Integral Equation for Viscous Fluids,' Proc. UTAM Conf. on BEM, San Antonio, Texas.

Mustoe, G.G.W. (1984), 'Advanced Integration Schemes Over Boundary Elements and Volume Cells for Two- and Three-dimensional Nonlinear Analysis,' in Developments in Boundary Element Methods - III, ed. P.K. Banerjee and S. Mukherjee, Applied Science Publishers, England.

Onishi, K. (1986), 'Boundary Element Analysis of Thermal Fluids Using ψ,ω' pp. 269-275 in R.P. Shaw et.al., Eds., Proc. 4th Intl. Symp. Innov. Num. Methods Engrg., Springer, Berlin.

Onishi, K., Kuroki, T., and Tanaka, ii. (1985), 'Boundary Element Method for Laminar Viscous Flow and Convective Diffusion Problems,' Chpt. 8 in C.A. Brebbia, Ed., Topics in B.E. Research, Springer, Berlin.

Onishi, K. and Kuroki, T. (1986), 'On Non-linear Heat Transfer Problems,' Chpt. 6 in P.K. Banerjee and J.O. Watson, Eds., Developments in B.E.M. - 4, Elsevier, London.

Piva, R., Graziani, G. and Morino, L. (1987) 'Boundary Integral Equation Method for Unsteady Viscous and Inviscid Flows,' IUTAM Symposium on Advanced Boundary Element Method, San Antonio, Texas.

Raveendra, S.T. (1984), Advanced Development for BEM for Two and Three Dimensional Nonlinear Analysis, Ph.D. Dissertation, State University of New York at Buffalo.

Sankar, N.L., and Wu. J.C. (1978), 'Viscous Flow Around on Oscillating Airfoil - A Numerical Study,' in AIAA 11th Fluid and Plasma Dyn. Conf., Seattle, Washington.

Stroud, A.H. and Secrest, D. (1966), Gaussian Quadrature Formulas, Prentice Hall, New York.

Tosaka, N. (1987) 'Integral Equation Method for Analysis of Newtonian and Non-Newtonian Flows', IUTAM Symposium on Advanced Boundary Element Method, San Antonio, Texas.

Tosaka, N., and Kakuda, K. (1986), 'Numerical Solutions of Steady Incompressible Viscous Flow Problems by Integral Equation Method,' pp. 211-222 in R.P. Shaw et.al., Eds., Proc. 4th Intl. Symp. Innov. Num. Methods Engrg., Springer, Berlin.

Tosaka, N. and Kakuda, K. (1987) 'Numerical Simulations of Laminar and Turbulent Flows by Using an Integral Equation,' Boundary Elements IX, eds. Brebbia, Wendland and Kuhn, pp. 489-502.

Wilson, R.B., Bak, M.J., Nakazawa, S., and Banerjee, P.K. (1984), '3-D Inelastic Analysis Methods for Hot Section Components (Base Program),' First Annual Status Report for the Period (Feb. 1983 to Feb. 1984), NASA Contractor Report 174700.

Wilson, R.B., Bak, M.J., Nakazawa, S., and Banerjee, P.K. (1985), '3-D Inelastic Analysis Methods for Hot Section Components (Base Program),' Second Annual Status Report for the Period (Feb. 1984 to Feb. 1985), NASA Contractor Report.

Wu, J.C. (1976a) 'Numerical Boundary Conditions for Viscous Flow Problems', AIAA Journal, Vol. 14, No. 8, 1042-1049.

Wu, J.C. (1976b) 'Finite Element Solution of Flow Problems using Integral Representations', pp. 205-216 in Proc. 2nd Int. Symp. on Fin. Elem. Methods in Fluid Problems.

Wu, J.C. (1982), 'Problems of General Viscous Flow,' Chpt. 4 in P.K. Banerjee and R.P. Shaw, Eds., Developments in B.E.M. - 3, Elsevier, London.

Wu. J.C. (1984), 'Fundamental Solutions and Numerical Methods for Flow Problems,' Int. J., Num. Meth. Fluids, Vol. 4, 1985-201.

Wu., J.C., and Rizk, Y.M. (1978), 'Integral-Representation Approach for Time-Dependent Viscous Flows,' pp. 558-564 in Lecture Notes in Physics, Vol. 90, Springer, Berlin.

Wu, J.C., Rizk, Y.M., and Sankar, H.L. (1984), 'Problems of Time-Dependent Navier-Stokes Flow,' Chpt. 6 in P.K. Banerjee and S. Mukherjee, Eds., Developments in B.E.M. - 3, Elsevier, London.

Wu, J.C., and Sampath, S. (1976) 'A Numerical Study of Viscous Flow Around an Airfoil', AIAA Paper 76-337, AIAA, New York.

Wu, J.C., Sampath, S., and Sankar, N.L. (1978a), 'A Numerical Study of Unsteady Viscous Flows Around Airfoils,' pp. 24/1-18 in AGRAD Conf. Proc. No. 227.

Wu, J.C., Spring, A.H., and Sankar, N.L. (1974), 'A Flowfield Segmentation Method for the Numerical Solution of Viscous Flow Problems,' pp. 452-457 in Proc. 4th Intl. Conference on Num. Methods in Fluid Dynamics, Springer, Berlin.

Wu, J.C., and Sugavanam, A. (1978), 'Method for the Numerical Solution of Turbulent Flow Problems,' AIAA Journal, Vol. 16, No. 9, 948-955.

Wu, J.C., and Thompson, J.F. (1973), 'Numerical Solutions of Time-Dependent Incompressible Navier-Stokes Equations Using an Integro-Differential Formulation,' Comp. and Fluids, Vol. 1, 197-215.

Wu, J.C., Wahbah, M.M., and Sugavanam, A. (1978b), 'Numerical Solution of Unsteady Flow Problems Using Integro-Differential Approach,' pp. 245-252, in D.E. Crow and J.A. Miller, Eds., Nonsteady Fluid Dynamics, ASME, New York.

Yuan, S.W. (1967), 'Foundations of Fluid Mechanics,' Prentice-Hall, New Jersey.

APPENDIX B - KERNELS FOR THERMOELASTICITY

This appendix contains the detailed presentations of all the kernel functions utilized in the formulations contained in Section 3. Two-dimensional (plane strain) kernels are provided, based upon continuous source and force fundamental solutions. For time-dependent uncoupled quasistatic thermoelasticity the following relationships must be used to determine the proper form of the functions required in the boundary element discretization. That is,

$$G^n_{\alpha\beta}(X-\xi) = G_{\alpha\beta}(X-\xi, n\Delta t) \qquad \text{for } n=1$$

$$G^n_{\alpha\beta}(X-\xi) = G_{\alpha\beta}(X-\xi, n\Delta t) - G_{\alpha\beta}(X-\xi, (n-1)\Delta t) \qquad \text{for } n>1 \ ,$$

with similar expressions holding for all the remaining kernels. In the specification of these kernels below, the arguments $(X-\xi,t)$ are assumed. The indices

i,j,k,l	vary from 1 to d
α,β	vary from 1 to (d+1)
θ	equals d+1

where d is the dimensionality of the problem. Additionally,

x_i	coordinates of integration point
ξ_i	coordinates of field point

$y_i = x_i - \xi_i \qquad r^2 = y_i y_i$.

For the displacement kernel,

$$G_{ij} = \frac{1}{8\pi} \frac{1}{\mu(1-\nu)} \left[\left(\frac{y_i y_j}{r^2}\right) - (\delta_{ij}) \ (3-4\nu) \ln r \right]$$

$$G_{i\theta} = 0$$

$$G_{\theta j} = \frac{r}{2\pi} \left(\frac{\beta}{k(\lambda+2\mu)}\right) \left[\left(\frac{y_j}{r}\right) \bar{g}_4(\eta) \right]$$

$$G_{\theta\theta} = \frac{1}{2\pi} \left(\frac{1}{k}\right) \left[\bar{g}_5(\eta) \right]$$

whereas, for the traction kernel,

$$F_{ij} = \frac{1}{4\pi r} \frac{1}{(1-\nu)} \left[-\left(\frac{2y_i y_j y_k n_k}{r^3}\right) - \left(\frac{\delta_{ij} y_k n_k + y_i n_j}{r}\right) (1-2\nu) \right.$$

$$\left. + \left(\frac{y_j n_i}{r}\right) (1-2\nu) \right]$$

$$F_{i\theta} = 0$$

$$F_{\theta j} = \frac{1}{4\pi} \left(\frac{\beta}{\lambda+2\mu}\right) \left[\left(\frac{y_j y_k n_k}{r^2}\right) \bar{f}_6(\eta) - (n_j) \bar{f}_7(\eta) \right]$$

$$F_{\theta\theta} = \frac{1}{2\pi r} \left[\left(\frac{y_k n_k}{r}\right) \bar{f}_8(\eta) \right] .$$

In the above,

$$\eta = \frac{r}{(ct)^{1/2}}$$

$$c = \frac{k}{\rho c_\varepsilon}$$

$$E_1(z) = \int_z^\infty \frac{e^{-x}}{x} \, dx$$

$$\bar{h}_1(\eta) = \frac{4}{\eta^2} \left(1-e^{-\eta^2/4}\right)$$

$$\bar{g}_4(\eta) = \frac{\bar{h}_1(\eta)}{2} + \frac{E_1(\frac{\eta^2}{4})}{2}$$

$$\bar{g}_5(\eta) = \frac{E_1(\frac{\eta^2}{4})}{2}$$

$$\bar{f}_6(\eta) = \bar{h}_1(\eta)$$

$$\bar{f}_7(\eta) = \frac{\bar{h}_1(\eta)}{2} + \frac{E_1(\frac{\eta^2}{4})}{2}$$

$$\bar{f}_8(\eta) = e^{-\eta^2/4} .$$

For the interior stress kernels,

$$E_{\beta ij} = \frac{2\mu\nu}{1-2\nu}\,\delta_{ij}\,\frac{\partial G_{\beta l}}{\partial \xi_l} + \mu\,(\frac{\partial G_{\beta i}}{\partial \xi_j} + \frac{\partial G_{\beta j}}{\partial \xi_i}) - \beta\delta_{ij}\,G_{\beta\theta}$$

$$D_{\beta ij} = \frac{2\mu\nu}{1-2\nu}\,\delta_{ij}\,\frac{\partial F_{\beta l}}{\partial \xi_l} + \mu\,(\frac{\partial F_{\beta i}}{\partial \xi_j} + \frac{\partial F_{\beta j}}{\partial \xi_i}) - \beta\delta_{ij}\,F_{\beta\theta}$$

where

$$\frac{\partial G_{ij}}{\partial \xi_k} = \frac{1}{8\pi r}\,\frac{1}{\mu(1-\nu)}\,[\,(\frac{2y_iy_jy_k}{r^3} - \frac{\delta_{jk}y_i}{r} - \frac{\delta_{ik}y_j}{r})$$

$$+ (\frac{\delta_{ij}y_k}{r})\,\{(3-4\nu)\,]$$

$$\frac{\partial G_{\theta j}}{\partial \xi_k} = \frac{1}{4\pi}\,(\frac{\beta}{k(\lambda+2\mu)})\,[\,(\frac{y_jy_k}{r^2})\,\{\bar{h}_1\} - (\delta_{jk})\,\{\frac{\bar{h}_1}{2} + \frac{E_1}{2}\}\,]$$

$$\frac{\partial F_{ij}}{\partial \xi_k} = \frac{1}{4\pi r^2}\,\frac{1}{(1-\nu)}\,\Big[\,-\Big(\frac{4y_iy_jy_ky_ln_l}{r^4} - \frac{y_iy_jn_k}{r^2} - \frac{\delta_{jk}y_iy_ln_l}{r^2}$$

$$- \frac{\delta_{ik}y_jy_ln_l}{r^2}\Big)\bar{f}_1(\eta)\,-\Big(\frac{2\delta_{ij}y_ky_ln_l}{r^2} - \delta_{ij}n_k + \frac{2y_iy_kn_j}{r^2} - \delta_{ik}n_j\Big)\bar{f}_2(\eta)$$

$$+ \Big(\frac{2y_jy_kn_i}{r^2} - \delta_{jk}n_i\Big)\bar{f}_3(\eta)\,\Big]$$

$$\frac{\partial F_{\theta j}}{\partial \xi_k} = \frac{1}{4\pi r}\,\Big(\frac{\beta}{\lambda+2\mu}\Big)\,\Big[\,\Big(\frac{2y_jy_ky_ln_l}{r^3}\Big)\{2\bar{h}_1 - e^{-\eta^2/4}\}$$

$$- \Big(\frac{y_kn_j}{r} + \frac{y_jn_k}{r} + \frac{\delta_{jk}y_ln_l}{r}\Big)\{\bar{h}_1\}\,\Big]\,.$$

$$\bar{f}_1(\eta) = 2$$

$$\bar{f}_2(\eta) = 1-2\nu$$

$$\bar{f}_3(\eta) = 1-2\nu$$

APPENDIX C - KERNELS FOR VISCOUS, INCOMPRESSIBLE FLOW

This appendix contains details of the time-dependent incompressible kernels necessary for the integral formulations of Section 4. Notation is consistent with that defined in Appendix B.

For the generalized velocity kernels,

$$G_{ij} = \frac{1}{4\pi\mu}\left[\left(\frac{y_i y_j}{r^2}\right) \{s_1(\varepsilon) - (\delta_{ij}) \left\{\frac{s_1(\varepsilon)}{2} - \frac{E_1(\frac{\varepsilon}{4})^2}{2}\right\} \right]$$

$$G_{i\theta} = 0$$

$$G_{\theta j} = 0$$

$$G_{\theta\theta} = \frac{1}{2\pi}\left(\frac{1}{k}\right)\left[\frac{E_1(\frac{\eta}{4})^2}{2} \right]$$

whereas, for the generalized traction kernel,

$$F_{ij} = \frac{1}{2\pi r}\left[\left(\frac{y_i n_j}{r}\right) \{s_1 - e^{-\varepsilon^2/4}\} + \left(\frac{\delta_{ij} y_k n_k}{r}\right) \{s_1 - e^{-\varepsilon^2/4}\} \right.$$

$$\left. - \left(\frac{y_j n_i}{r}\right) \{H(t) - s_1\} - \left(\frac{2 y_i y_j y_k n_k}{r^3}\right) \{2s_1 - e^{-\varepsilon^2/4}\} \right]$$

$$F_{i\theta} = 0$$

$$F_{\theta j} = 0$$

$$F_{\theta\theta} = \frac{1}{2\pi r}\left[\left(\frac{y_k n_k}{r}\right) e^{-\eta^2/4} \right].$$

In the above,

$$\varepsilon = \frac{r}{(c't)^{1/2}}$$

$$c' = \frac{\mu}{\rho}$$

$$s_1(\varepsilon) = \frac{4}{\varepsilon^2}\,(1-e^{-\varepsilon^2/4})$$

$$\eta = \frac{r}{(ct)^{1/2}}$$

$$c = \frac{k}{\rho c_\varepsilon}$$

$$E_1(z) = \int_z^\infty \frac{e^{-u}}{u}\,du$$

Meanwhile, for the interior strain rates,

$$E_{ijk} = \frac{1}{4\pi r}\left(\frac{1}{\mu}\right)\left[- \left(\frac{\delta_{jk}y_i}{r}\right)\{s_1\} - \left(\frac{\delta_{ik}y_j}{r}\right)\{s_1\} + \left(\frac{2y_iy_jy_k}{r^3}\right)\{2s_1-e^{-\varepsilon^2/4}\}\right.$$

$$\left. + \left(\frac{\delta_{ij}y_k}{r}\right)\{2e^{-\varepsilon^2/4}-s_1\}\right]$$

$$D_{ijk} = \frac{1}{2\pi r^2}\left[- \left(\frac{y_iy_jy_ky_mn_m}{r^4}\right)\bar{g}_1 - \left(\frac{\delta_{ij}y_ky_mn_m}{r^2} + \frac{y_iy_kn_j}{r^2}\right)\bar{g}_2 + \left(\frac{y_jy_kn_i}{r^2}\right)\bar{g}_3\right.$$

$$+ \left(\frac{y_iy_jn_k}{r^2} + \frac{\delta_{jk}y_iy_mn_m}{r^2} + \frac{\delta_{ik}y_jy_mn_m}{r^2}\right)g_1$$

$$\left. + (\delta_{ij}n_k + \delta_{ik}n_j)g_2 - (\delta_{jk}n_i)g_3\right]$$

where

$$g_1 = 4s_1 - 2e^{-\varepsilon^2/4}$$

$$g_2 = -s_1 + e^{-\varepsilon^2/4}$$

$$g_3 = H(t) - s_1$$

$$\bar{g}_1 = 24s_1 - 16e^{-\eta^2/4} - \varepsilon^2 e^{-\varepsilon^2/4}$$

$$\bar{g}_2 = -4s_1 + re^{-\varepsilon^2/4} + \frac{\varepsilon^2}{2} e^{-\varepsilon^2/4}$$

$$\bar{g}_3 = 4s_1 - 2e^{-\varepsilon^2/4} - 2H(t).$$